Robust Formation Control and Obstacle Avoidance for Heterogeneous Underactuated Surface Vessel Networks

Bo Wang, *Graduate Student Member, IEEE*, Sergey G. Nersesov, *Member, IEEE*, and Hashem Ashrafiuon, *Senior Member, IEEE*

***Abstract*—This article investigates distributed robust formation control and distributed obstacle avoidance problems for networks of heterogeneous underactuated surface vessels without global position measurements. We exploit the cascaded structure of the kinematics and dynamics of generic vessel models to develop structured reduced-order error dynamics for group cooperation. By incorporating graph theory, the supertwisting control technique, and persistence of excitation concept, a distributed robust formation control scheme is developed without requiring global position measurements, where agents in the network may possess completely different dynamic models. It is shown that the stabilization of the reduced-order error dynamics guarantees the stability of the entire vessel error system subject to modeling uncertainties and bounded disturbances. Distributed obstacle avoidance is achieved by surrounding obstacles with stable elliptical limit cycles. During the obstacle avoidance stage, a part of the formation deforms to allow vessels to follow transient trajectories around static and dynamic obstacles. Simulation results are provided to demonstrate that the proposed cooperative control scheme can prevent obstacle and interagent collisions while achieving robust formation in heterogeneous underactuated vessel networks.**

***Index Terms*—Distributed obstacle avoidance, heterogeneous networks, robust formation control, underactuated marine vehicles.**

I. Introduction

A. Motivation and Related Works

THE FORMATION control problem of multivehicle networks has attracted great attention within the fields of control engineering and marine industry in recent decades due to increasing potential military and civilian applications [1], [2]. A network of marine vehicles can be used for significant and practical tasks such as reconnaissance, mine clearance, marine search, and rescue missions, to name a few. Such tasks cannot be performed by a single vehicle due to its limited capability and vulnerability to malfunctions. However, operating multiple vehicles as a team can enhance efficiency and increase robustness to individual agent failures.

The distributed formation control problem consists of making all the agents form a predefined geometrical configuration through *local* interactions. In other words, each follower uses only *local* information, e.g., relative position measurements, to achieve a *global* formation task. Other topics of cooperative control, such as consensus, swarm, collective tracking, and containment control of multivehicle systems, are also closely related to formation control. Various formation control schemes have been proposed, such as leader-follower strategy [3], virtual structure method [4], and behavior-based approach [5]. Among these formation control schemes, the leader–follower strategy is particularly appreciated in many applications for its simplicity and scalability [3].

Numerous formation control designs for underactuated surface vessels using the leader–follower strategy can be found in the literature [2], [6]–[14]. In [6], sliding mode formation controllers have been proposed for unmanned surface vessels based on two specific geometric schemes. In [8], position-based cooperative control laws for underactuated surface vessels have been proposed for different communication scenarios. In [9], using generalized saturation functions, formation control laws with limited torque are presented to reduce the risk of actuator saturation. Using time-varying *tan*-type barrier Lyapunov functions, a fault-tolerant leader–follower formation control scheme was proposed in [2] for a class of underactuated surface vessels with line-of-sight range and angle constraints. Then, Ghommam and Saad [10] generalized the result in [2] to asymmetric time-varying constraints on the range and bearing angle between the follower and the leader in the formation. In [11], based on sliding mode control and parameter estimation, a leader–follower formation control law was proposed for surface vessels with model uncertainties and environmental disturbances. A finite-time formation control design is presented for underactuated ships based on terminal sliding mode theory in [12]. In [13], practical formation-containment tracking protocols are designed based on extended state observers. Recently, in [14], using neural

Manuscript received July 10, 2021; revised July 15, 2021 and November 16, 2021; accepted November 29, 2021. Date of publication January 6, 2022; date of current version May 26, 2022. This work was supported by the U.S. Office of Naval Research under Grant N00014-19-1-2255. Recommended by Associate Editor Alexander Olshevsky. *(Corresponding author: Hashem Ashrafiuon.)*

The authors are with the Department of Mechanical Engineering, Villanova University, Villanova, PA 19085 USA (e-mail: bwang6@villanova.edu; sergey.nersesov@villanova.edu; hashem.ashrafiuon@villanova.edu).

Digital Object Identifier 10.1109/TCNS.2022.3141022

networks and high-gain observers, an adaptive output-feedback formation control law was developed for vessels without velocity measurements.

Although numerous formation control schemes have been proposed for underactuated surface vessels in the literature, there are several common drawbacks in the existing controllers. First, surface vessels in practical applications may have different parameters or even different dynamical models due to the various sizes, shapes, and loads. The vessels in the network may be described by different models such as diagonal or coupled mass matrix model and linear or nonlinear hydrodynamic damping model [15]. Thus, it is more practical if a group of vessels can cooperate with each other regardless of the parameters or even structures of their dynamical models. In other words, we need formation control schemes developed for *heterogeneous* networks. However, in [6], [8], [10], and [12]–[14], not only the dynamical model structure but also the parameters of all the vessels in the network are required to be identical, which is a very strict and unrealistic assumption. Second, in contrast to the *displacement-based* approach, in the position-based control scheme such in [8] and [9], vessels need to sense their global positions with respect to a global coordinate system. In this case, the communications among agents are unnecessary since the desired formation can be achieved by position control of individual vessels [16]. Furthermore, using global sensors could be quite a demanding requirement depending upon the environment and could be biased easily due to measurement errors [17]. On the other hand, the displacement-based approach balances the sensing capability and the interaction requirements, and it is particularly appreciated in many applications, especially in situations when the GPS signal is not available, while onboard sensors can provide measurements necessary for feedback control design. It is certain that if the agents have distributed sensing capabilities, they can control themselves based on *local* interactions. Therefore, to improve the cooperative ability, traffic safety, and communication efficiency, it is preferable to have vessel-to-vessel interactions and to control the intervessel configurations using onboard vehicle sensors. Third, as pointed in [11], static or time-varying obstacle avoidance capability should be taken into account in the controller design in practical applications.

B. Main Contributions

The main contribution and novelty of this article is in designing a distributed robust formation control framework with distributed obstacle avoidance capability for networks of heterogeneous underactuated surface vessels using only neighbor-to-neighbor information exchange.

1) We solve the robust formation control problem for *heterogeneous* underactuated vessel networks. In other words, we do not assume any particular structure of the internal dynamics of each vehicle but rather use a generic dynamical model, and the vehicles in the network are allowed to have identical or nonidentical dynamics.
2) We solve the *obstacle avoidance* problem using a simple distributed strategy that surrounds obstacles with stable elliptical limit cycles and forces the vessels to converge to the limit cycle solutions. It should be noted that our distributed obstacle avoidance capability also includes *collision avoidance* among the network agents.
3) Both the proposed formation control law and obstacle avoidance control law require only *neighbor-to-neighbor* information exchange and do not require any global position measurements of the followers. We emphasize that not requiring "global position measurements" is an essential difficulty in distributed control.

We also emphasize that in contrast to cooperative control of heterogeneous fully actuated systems, the problem of cooperative control of heterogeneous *underactuated* systems is far more complex. This is not only because the number of independent actuators is less than the number of degrees of freedom and thus have limited capability, but also because all fully actuated systems are feedback equivalent to double-integrator dynamics, and hence, the problem of cooperative control of heterogeneous fully actuated systems is equivalent to cooperative control of homogeneous double-integrator agents. To the best of the authors' knowledge, this is the first work that solves the heterogeneous formation control problem *without* requiring any particular structure of the internal dynamics of the underactuated vehicles and *without* requiring any global position measurement. This article is the continuation of earlier work on formation control of homogeneous underactuated surface vessel networks [18] extended to heterogeneous networks with distributed obstacle avoidance ability and a new control design.

II. Preliminaries and Problem Formulation

A. Notations

Let $\mathbb{R}^n$ represent the n-dimensional Euclidean space, $\mathbb{R}_{\geq 0}$ the set of all nonnegative real numbers, $|x|$ the Euclidean norm of a vector $x \in \mathbb{R}^n$, $\text{diag}\{\cdot\} \in \mathbb{R}^{n\times n}$ the diagonal matrix, $\mathcal{L}_2$ the space of all square integrable functions, and $\mathcal{L}_\infty$ the space of all essentially bounded functions. For a bounded and piecewise continuous function $u : \mathbb{R} \to \mathbb{R}^n$, let $|u|_\infty$ denote its sup norm. For any two convergent functions $f_1(t)$ and $f_2(t)$, we use $f_1(t) \to f_2(t)$ to represent $|f_1(t) - f_2(t)| \to 0$ as $t \to \infty$, and use $\xrightarrow{\text{exp}}$ to represent the exponential convergence. Throughout this article, we omit the arguments of functions when they are clear from the context. In the context of multiagent systems, we use the bold and nonitalicized subscript $\mathbf{i}$ to denote the index of an agent.

B. Model Description

Consider a network of $N+1$ heterogeneous underactuated surface vessels where the vessels are numbered $\mathbf{i} = 0, 1, \ldots, N$ with $\mathbf{1}, \ldots, \mathbf{N}$ representing all the followers and $\mathbf{0}$ the (virtual or real) group leader. The motion of a single vessel $\mathbf{i}$ in the network is described by assigning a body-fixed reference frame $\{x_{b\mathbf{i}} y_{b\mathbf{i}}\}$ to its center of mass located at $(x_\mathbf{i}, y_\mathbf{i}) \in \mathbb{R}^2$ with respect to a fixed inertial reference frame $\{XY\}$ and yaw angle $\theta_\mathbf{i} \in \mathbb{R}$, as shown in Fig. 1. Note that most practical surface vessels, including unmanned ones, have two actual inputs, which can be

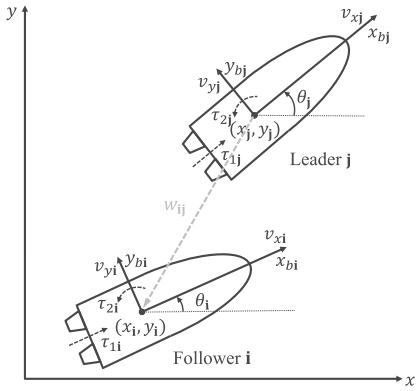

Fig. 1. Top view of the leader–follower formation of underactuated surface vessels $\mathbf{i}$ and $\mathbf{j}$.

mapped into the surge and yaw control inputs. We assume that each vessel in the network has only two actuators, which provide the surge control force and the yaw control moment.

The mathematical model of the vessel is represented by its kinematics and generic planar rigid body dynamics

$$\begin{cases} \dot{x}_{\mathbf{i}} = v_{x\mathbf{i}} \cos\theta_{\mathbf{i}} - v_{y\mathbf{i}} \sin\theta_{\mathbf{i}} \\ \dot{y}_{\mathbf{i}} = v_{x\mathbf{i}} \sin\theta_{\mathbf{i}} + v_{y\mathbf{i}} \cos\theta_{\mathbf{i}} \\ \dot{\theta}_{\mathbf{i}} = \omega_{\mathbf{i}} \end{cases} \tag{1a}$$

$$\begin{cases} \dot{v}_{x\mathbf{i}} = f_{x\mathbf{i}}(v_{x\mathbf{i}}, v_{y\mathbf{i}}, \omega_{\mathbf{i}}) + \delta_{x\mathbf{i}}(v_{x\mathbf{i}}, v_{y\mathbf{i}}, \omega_{\mathbf{i}}, \theta_{\mathbf{i}}, t) + \tau_{1\mathbf{i}} \\ \dot{v}_{y\mathbf{i}} = f_{y\mathbf{i}}(v_{x\mathbf{i}}, v_{y\mathbf{i}}, \omega_{\mathbf{i}}) + \delta_{y\mathbf{i}}(v_{x\mathbf{i}}, v_{y\mathbf{i}}, \omega_{\mathbf{i}}, \theta_{\mathbf{i}}, t) \\ \dot{\omega}_{\mathbf{i}} = f_{\omega\mathbf{i}}(v_{x\mathbf{i}}, v_{y\mathbf{i}}, \omega_{\mathbf{i}}) + \delta_{\omega\mathbf{i}}(v_{x\mathbf{i}}, v_{y\mathbf{i}}, \omega_{\mathbf{i}}, \theta_{\mathbf{i}}, t) + \tau_{2\mathbf{i}} \end{cases} \tag{1b}$$

where $(v_{x\mathbf{i}}, v_{y\mathbf{i}})$ represents the velocity of the center of mass of vessel $\mathbf{i}$ in the body-fixed frame $\{x_{b\mathbf{i}} y_{b\mathbf{i}}\}$, and $\omega_{\mathbf{i}}$ is its angular velocity. Functions $f_{x\mathbf{i}}(\cdot), f_{y\mathbf{i}}(\cdot)$, and $f_{\omega\mathbf{i}}(\cdot)$ are known locally as Lipschitz continuous functions, which usually consist of nominal inertial, Coriolis-like, and hydrodynamic damping terms. The terms $\delta_{x\mathbf{i}}(\cdot), \delta_{y\mathbf{i}}(\cdot), \delta_{\omega\mathbf{i}}(\cdot)$ represent the unknown terms, which may include modeling uncertainties and bounded disturbances with bounded first derivatives, i.e.,

$$\begin{aligned} \max\{|\delta_{x\mathbf{i}}(\cdot)|_\infty, |\dot{\delta}_{x\mathbf{i}}(\cdot)|_\infty\} &\le \Delta_{x\mathbf{i}} \\ \max\{|\delta_{y\mathbf{i}}(\cdot)|_\infty, |\dot{\delta}_{y\mathbf{i}}(\cdot)|_\infty\} &\le \Delta_{y\mathbf{i}} \\ \max\{|\delta_{\omega\mathbf{i}}(\cdot)|_\infty, |\dot{\delta}_{\omega\mathbf{i}}(\cdot)|_\infty\} &\le \Delta_{\omega\mathbf{i}} \end{aligned} \tag{2}$$

where $\Delta_{x\mathbf{i}}, \Delta_{y\mathbf{i}}, \Delta_{\omega\mathbf{i}}$ are known positive constants. In this work, all potential parametric uncertainties can be lumped into the terms $\delta_{x\mathbf{i}}(\cdot), \delta_{y\mathbf{i}}(\cdot), \delta_{\omega\mathbf{i}}(\cdot)$. Control inputs $\tau_{1\mathbf{i}}$ and $\tau_{2\mathbf{i}}$ represent scaled surge force and yaw moment, respectively, as shown in Fig. 1. We assume that the (virtual or real) group leader can also be represented by the model (1a), (1b), and its state vector $(x_{\mathbf{0}}, y_{\mathbf{0}}, \theta_{\mathbf{0}}, v_{x\mathbf{0}}, v_{y\mathbf{0}}, \omega_{\mathbf{0}})$ is assumed to be bounded with a bounded first derivative for all $t \ge 0$.

From rigid body dynamics, the term $f_{y\mathbf{i}}(\cdot)$ in the sway force-balance equation of (1b) in body-fixed frame consists of inertial force terms $f^{\mathrm{C}}_{y\mathbf{i}}(\cdot)$ and damping terms $f^{\mathrm{D}}_{y\mathbf{i}}(\cdot)$, i.e., $f_{y\mathbf{i}} = f^{\mathrm{C}}_{y\mathbf{i}} + f^{\mathrm{D}}_{y\mathbf{i}}$. The inertial force terms $f^{\mathrm{C}}_{y\mathbf{i}}(\cdot)$ are quadratic in velocity such that the component in the $y_{b\mathbf{i}}$-direction is only a function of $v_{x\mathbf{i}}$ and $\omega_{\mathbf{i}}$, i.e., $f^{\mathrm{C}}_{y\mathbf{i}} = f^{\mathrm{C}}_{y\mathbf{i}}(v_{x\mathbf{i}}, \omega_{\mathbf{i}})$, and always points to the negative $y_{b\mathbf{i}}$-direction such that

$$\frac{\partial f^{\mathrm{C}}_{y\mathbf{i}}}{\partial v_{x\mathbf{i}}}(\omega_{\mathbf{i}}) = -\eta_{\mathbf{i}}\omega_{\mathbf{i}}, \eta_{\mathbf{i}} > 0.$$

Furthermore, the component of the hydrodynamic damping force along the $y_{b\mathbf{i}}$-axis is only related to $v_{y\mathbf{i}}$, i.e., $f^{\mathrm{D}}_{y\mathbf{i}} = f^{\mathrm{D}}_{y\mathbf{i}}(v_{y\mathbf{i}})$, and its direction is always opposite to $v_{y\mathbf{i}}$ such that $\frac{\partial f^{\mathrm{D}}_{y\mathbf{i}}}{\partial v_{y\mathbf{i}}}(v_{y\mathbf{i}}) \le 0$.

C. Notions From Graph Theory

We use graph theory to define the communication network among the vessels of the network. Network topology of the $N+1$ surface vessels is defined by a digraph $\mathcal{G} = (\mathcal{V}, \mathcal{E})$ where $\mathcal{V} = \{\mathbf{0}, \mathbf{1}, \ldots, \mathbf{N}\}$ and $\mathcal{E} \subseteq \mathcal{V} \times \mathcal{V}$ represent its sets of vertices and edges, respectively. There are $N+1$ nodes whose node dynamics are described in (1a), (1b). The set of neighboring nodes with edges connected to node $\mathbf{i}$ is denoted by $\Omega_{\mathbf{i}} = \{\mathbf{j} \mid (\mathbf{i}, \mathbf{j}) \in \mathcal{E}\}$. The edges represent communication between the nodes such that (follower) node $\mathbf{i}$ can obtain information from (leader) node $\mathbf{j}$ for feedback control purposes, if $\mathbf{j} \in \Omega_{\mathbf{i}}$, as shown in Fig. 1. Here, we use the terms "leader" and "follower" only to distinguish between agents that send information and those that receive them. In order to incorporate a combination of neighboring feedback information from neighboring nodes, we let $w_{\mathbf{ij}}$ be a nonnegative constant weighing factor for any $\mathbf{i}, \mathbf{j} \in \mathcal{V}$. These factors are selected such that $\sum_{\mathbf{j} \in \Omega_{\mathbf{i}}} w_{\mathbf{ij}} = 1$ if $(\mathbf{i}, \mathbf{j}) \in \mathcal{E}$, and $w_{\mathbf{ij}} = 0$ otherwise. We assume that there exists at least one directed path starting from the group leader $\mathbf{0}$ to any other node in the network, which implies that graph $\mathcal{G}$ contains a directed spanning tree [19]. We also assume there is no loop in $\mathcal{G}$, and the group leader does not receive any communication from other nodes. For more details on algebraic graph theory, see [19].

D. Problem Formulation

The objective of distributed formation control is to design a controller for each agent such that it coordinates its motion relative to its neighbors, and the network asymptotically converges to a predefined geometric pattern. Moreover, during this coordinated motion, each agent should be able to bypass any obstacle and avoid collisions with other agents. The desired geometric pattern of vessel network in terms of planar positions is defined by a set of constant position offset vectors $\{(d^x_{\mathbf{ij}}, d^y_{\mathbf{ij}}) \in \mathbb{R}^2 : \mathbf{i}, \mathbf{j} \in \mathcal{V},\ \mathbf{i} \ne \mathbf{j}\}$. Furthermore, each obstacle considered in this article is assumed to be surrounded by an ellipse described by the equation $l_{\mathbf{o}}(t, \chi_1, \chi_2)=0$, where $\mathbf{o}$ is the obstacle number

$$l_{\mathbf{o}} = \left[\frac{\chi_1 \cos\phi_{\mathbf{o}} + \chi_2 \sin\phi_{\mathbf{o}}}{a_{\mathbf{o}}}\right]^2 + \left[\frac{\chi_2 \cos\phi_{\mathbf{o}} - \chi_1 \sin\phi_{\mathbf{o}}}{b_{\mathbf{o}}}\right]^2 - 1$$

$\chi_1 = x - x_{\mathbf{o}}(t)$ and $\chi_2 = y - y_{\mathbf{o}}(t)$. $(x_{\mathbf{o}}(t), y_{\mathbf{o}}(t))$ denotes the position of the ellipse center in the global frame, $\phi_{\mathbf{o}}(t)$ is the ellipse orientation angle, and $a_{\mathbf{o}}$ and $b_{\mathbf{o}}$ are the semimajor and semiminor axes of the ellipse, respectively. Specifically, we will solve the following two problems.

Robust formation control problem: Design control laws $\tau_{1\mathbf{i}}, \tau_{2\mathbf{i}}$ for each $\mathbf{i}$th follower without global position measurements such that:

1) all states in the closed-loop system are uniformly bounded for all $t \geq 0$;
2) all the vessels in the network can maintain a prescribed formation in the sense that

$$\lim_{t\to\infty} \left| \sum_{\mathbf{j}\in\Omega_\mathbf{i}} w_{\mathbf{ij}} \begin{bmatrix} x_\mathbf{i}(t) - x_\mathbf{j}(t) - d^x_{\mathbf{ij}} \\ y_\mathbf{i}(t) - y_\mathbf{j}(t) - d^y_{\mathbf{ij}} \end{bmatrix} \right| = 0; \tag{3}$$

3) all bounded modeling uncertainties and disturbances can be rejected or attenuated in the closed-loop system.

Distributed obstacle avoidance problem: Design control laws $\tau_{1\mathbf{i}}, \tau_{2\mathbf{i}}$ for each $\mathbf{i}$th follower without global position measurements such that the $\mathbf{i}$th follower is able to bypass any (moving) $\mathbf{o}$th obstacle on its path in the sense that

$$l_\mathbf{o}(t, \tilde{x}_{\mathbf{io}}, \tilde{y}_{\mathbf{io}}) > 0 \;\; \forall t \geq 0 \tag{4}$$

where $(\tilde{x}_{\mathbf{io}}, \tilde{y}_{\mathbf{io}}) = (x_\mathbf{i}(t) - x_\mathbf{o}(t), y_\mathbf{i}(t) - y_\mathbf{o}(t))$ is the relative position error.

Remark 1: In general, the network position offsets may be smooth time-varying vectors $(d^x_{\mathbf{ij}}(t), d^y_{\mathbf{ij}}(t))$, making the formation time varying. Although, in this article, we focus on time-invariant formations, all the results can be easily generalized to the case of time-varying formations. This, however, is omitted in our discussion to simplify the notation and derivations. Moreover, the condition (4) implies that the $\mathbf{i}$th vessel will never enter the $\mathbf{o}$th elliptical region and, thus, will never touch the obstacle on its path.

E. Feasible Reference Trajectories Generation

Due to the underactuated nature of surface vessels, the reference pose trajectory dictated by the formation cannot be arbitrarily assigned for each $\mathbf{i}$th follower. That is, given the relative pose measurements $(x_\mathbf{i}(t) - x_\mathbf{j}(t), y_\mathbf{i}(t) - y_\mathbf{j}(t), \theta_\mathbf{i}(t) - \theta_\mathbf{j}(t))$ and the desired formation pose offset vectors $(d^x_{\mathbf{ij}}, d^y_{\mathbf{ij}}, d^\theta_{\mathbf{ij}})$, where $\mathbf{j} \in \Omega_\mathbf{i}$ and $d^\theta_{\mathbf{ij}}$ denotes the desired orientation offset between the $\mathbf{i}$th and $\mathbf{j}$th agents, the feasible *orientation* trajectory must be determined based on the vessel model. For illustration, let us denote the position reference trajectory for the $\mathbf{i}$th vessel by

$$\bar{x}_\mathbf{i}(t) := \sum_{\mathbf{j}\in\Omega_\mathbf{i}} w_{\mathbf{ij}} \left[x_\mathbf{j}(t) + d^x_{\mathbf{ij}}\right], \bar{y}_\mathbf{i}(t) := \sum_{\mathbf{j}\in\Omega_\mathbf{i}} w_{\mathbf{ij}} \left[y_\mathbf{j}(t) + d^y_{\mathbf{ij}}\right].$$

Then, the feasible orientation trajectory $\bar{\theta}_\mathbf{i}(t)$ is forced to obey the same second-order nonholonomic constraint of the $\mathbf{i}$th vessel. Thus, the feasible orientation trajectory $\bar{\theta}_\mathbf{i}(t)$ is the solution to the second equation in (1b), which is a first-order ordinary differential equation with respect to $\bar{\theta}_\mathbf{i}(t)$

$$\dot{\bar{v}}_{y\mathbf{i}}(t) = f_{y\mathbf{i}}\left(\bar{v}_{x\mathbf{i}}(t), \bar{v}_{y\mathbf{i}}(t), \dot{\bar{\theta}}_\mathbf{i}(t)\right) \tag{5}$$

subjected to the initial condition $\bar{\theta}_\mathbf{i}(0) = \bar{\theta}_{\mathbf{i},0}$. The terms $\bar{v}_{x\mathbf{i}}(t)$ and $\bar{v}_{y\mathbf{i}}(t)$ are derived from the kinematic model (1a)

$$\begin{bmatrix} \bar{v}_{x\mathbf{i}}(t) \\ \bar{v}_{y\mathbf{i}}(t) \end{bmatrix} = \begin{bmatrix} \cos\bar{\theta}_\mathbf{i}(t) & \sin\bar{\theta}_\mathbf{i}(t) \\ -\sin\bar{\theta}_\mathbf{i}(t) & \cos\bar{\theta}_\mathbf{i}(t) \end{bmatrix} \begin{bmatrix} \dot{\bar{x}}_\mathbf{i}(t) \\ \dot{\bar{y}}_\mathbf{i}(t) \end{bmatrix}$$

with $\dot{\bar{x}}_\mathbf{i}(t) = \sum_{\mathbf{j}\in\Omega_\mathbf{i}} w_{\mathbf{ij}} \dot{x}_\mathbf{j}(t)$ and $\dot{\bar{y}}_\mathbf{i}(t) = \sum_{\mathbf{j}\in\Omega_\mathbf{i}} w_{\mathbf{ij}} \dot{y}_\mathbf{j}(t)$. Therefore, the feasible orientation trajectory $\bar{\theta}_\mathbf{i}(t)$ is obtained by numerically integrating (5) in real time given the position offset $(d^x_{\mathbf{ij}}, d^y_{\mathbf{ij}})$. Finally, the feasible orientation offset $d^\theta_{\mathbf{ij}}$ is selected as $d^\theta_{\mathbf{ij}}(t) := \bar{\theta}_\mathbf{i}(t) - \theta_\mathbf{j}(t)$.

As pointed out in Remark 1, the feasible reference trajectory generation procedure described above can also be used in the time-varying formation. In that case, the time-varying position offset $(d^x_{\mathbf{ij}}(t), d^y_{\mathbf{ij}}(t))$ should be a smooth function, and all the remaining feasible trajectory generation procedures are the same. It is noted that only the time derivatives of $\bar{x}_\mathbf{i}(t)$ and $\bar{y}_\mathbf{i}(t)$ are used in the feasible reference trajectory generation, and the global position measurements $(x_\mathbf{j}(t), y_\mathbf{j}(t))$ are not required.

III. Formation Control Formulation

A. Reduced-Order Error Dynamics

Here, we introduce a velocity transformation that results in reduced-order error dynamics to simplify the formation control design. Let $q_\mathbf{i} := [x_\mathbf{i}, y_\mathbf{i}, \theta_\mathbf{i}]^\top$ represent the configuration vector of agent $\mathbf{i}$, $\bar{q}_\mathbf{i} := [\bar{x}_\mathbf{i}, \bar{y}_\mathbf{i}, \bar{\theta}_\mathbf{i}]^\top$ the reference trajectory, and $v_\mathbf{i} := [v_{x\mathbf{i}}, v_{y\mathbf{i}}, \omega_\mathbf{i}]^\top$ the velocity vector. It can be seen that if, for any $\mathbf{i}$th agent, $q_\mathbf{i}(t) \to \bar{q}_\mathbf{i}(t)$ as $t \to \infty$, then (5) holds. Thus, the formation error vector $z_\mathbf{i} = [z_{1\mathbf{i}}, z_{2\mathbf{i}}, z_{3\mathbf{i}}]^\top$ for agent $\mathbf{i}$ is defined using the following transformation:

$$z_\mathbf{i} := J\left(\theta_\mathbf{i}\right)\left[\left(\dot{q}_\mathbf{i} - \dot{\bar{q}}_\mathbf{i}\right) + \Lambda\left(q_\mathbf{i} - \bar{q}_\mathbf{i}\right)\right] \tag{6}$$

where $J(\theta_\mathbf{i})$ is the orthogonal rotation matrix

$$J(\theta_\mathbf{i}) := \begin{bmatrix} \cos\theta_\mathbf{i} & \sin\theta_\mathbf{i} & 0 \\ -\sin\theta_\mathbf{i} & \cos\theta_\mathbf{i} & 0 \\ 0 & 0 & 1 \end{bmatrix}$$

and $\Lambda = \mathrm{diag}\{\lambda_1, \lambda_2, \lambda_3\}$ is a positive definite matrix. The following lemma is needed for the main result of this section.

Lemma 1: Consider the formation error $z_\mathbf{i}(t)$ given in (6), where $\Lambda = \mathrm{diag}\{\lambda_1, \lambda_2, \lambda_3\}$ is a positive definite matrix. For the $\mathbf{i}$th follower agent, if $z_\mathbf{i}(t)$ is uniformly bounded for all $t \geq 0$ and $z_\mathbf{i} \to 0$ as $t \to \infty$, then the *robust formation control problem* is solved.

Proof: Since $J(\theta_\mathbf{i})$ is an orthogonal matrix, $z_\mathbf{i} \in \mathcal{L}_\infty$ implies $[(\dot{q}_\mathbf{i} - \dot{\bar{q}}_\mathbf{i}) + \Lambda(q_\mathbf{i} - \bar{q}_\mathbf{i})] \in \mathcal{L}_\infty$, and $z_\mathbf{i}(t) \to 0$ as $t \to \infty$ implies that $[(\dot{q}_\mathbf{i} - \dot{\bar{q}}_\mathbf{i}) + \Lambda(q_\mathbf{i} - \bar{q}_\mathbf{i})] \to 0$ as $t \to \infty$, which can be written as

$$\frac{\mathrm{d}}{\mathrm{d}t}(q_\mathbf{i} - \bar{q}_\mathbf{i}) = -\Lambda(q_\mathbf{i} - \bar{q}_\mathbf{i}) + o_\mathbf{i}(t), \quad \lim_{t\to\infty} o_\mathbf{i}(t) = 0 \tag{7}$$

where $o_\mathbf{i}(t) := J(\theta_\mathbf{i})^\top z_\mathbf{i}(t)$. Then from the converging-input converging-state property of stable linear systems[20, p. 59], we conclude that $(q_\mathbf{i}(t) - \bar{q}_\mathbf{i}(t))$ is uniformly bounded and the origin of (7) is asymptotically stable, which implies that $(q_\mathbf{i}(t) - \bar{q}_\mathbf{i}(t)) \to 0$ and $(\dot{q}_\mathbf{i}(t) - \dot{\bar{q}}_\mathbf{i}(t)) \to 0$ as $t \to \infty$. Since this convergence holds for all agents, we conclude that (3) holds. □

Referring to Lemma 1, the objective of formation tracking control design is to drive $z_\mathbf{i}(t)$ to zero asymptotically for all $\mathbf{i} = 1, \ldots, N$. The error dynamics in terms of $z_\mathbf{i}$ are determined

by taking the time derivative of (6)

$$\dot{z}_{\mathbf{i}} = \dot{J}\left[(\dot{q}_{\mathbf{i}} - \dot{\bar{q}}_{\mathbf{i}}) + \Lambda\left(q_{\mathbf{i}} - \bar{q}_{\mathbf{i}}\right)\right] + J\left[(\ddot{q}_{\mathbf{i}} - \ddot{\bar{q}}_{\mathbf{i}}) + \Lambda\left(\dot{q}_{\mathbf{i}} - \dot{\bar{q}}_{\mathbf{i}}\right)\right]. \tag{8}$$

Substituting (1a) and (1b) for the **i**th and **j**th agents into the error dynamics (8) and using the feedback transformation

$$\begin{aligned}\tau_{1\mathbf{i}} = &-f_{x\mathbf{i}} + c_{(\mathbf{i}-\bar{\mathbf{i}})}\left(\dot{\bar{v}}_{x\mathbf{i}} - \bar{\omega}_{\mathbf{i}}\bar{v}_{y\mathbf{i}}\right) + s_{(\mathbf{i}-\bar{\mathbf{i}})}\left(\dot{\bar{v}}_{y\mathbf{i}} + \bar{\omega}_{\mathbf{i}}\bar{v}_{x\mathbf{i}}\right)\\ &- \lambda_1[v_{x\mathbf{i}} - c_{(\mathbf{i}-\bar{\mathbf{i}})}\bar{v}_{x\mathbf{i}} - s_{(\mathbf{i}-\bar{\mathbf{i}})}\bar{v}_{y\mathbf{i}}] + \omega_{\mathbf{i}}v_{y\mathbf{i}} + u_{1\mathbf{i}} \qquad (9)\end{aligned}$$

$$\tau_{2\mathbf{i}} = -f_{\omega\mathbf{i}} + \dot{\bar{\omega}}_{\mathbf{i}} - \lambda_3\left(\omega_{\mathbf{i}} - \bar{\omega}_{\mathbf{i}}\right) + u_{2\mathbf{i}} \tag{10}$$

where $c_{(\mathbf{i}-\bar{\mathbf{i}})} = \cos(\theta_{\mathbf{i}} - \bar{\theta}_{\mathbf{i}})$ and $s_{(\mathbf{i}-\bar{\mathbf{i}})} = \sin(\theta_{\mathbf{i}} - \bar{\theta}_{\mathbf{i}})$, we derive the reduced-order error dynamics in the following simple *structured* form:

$$\dot{z}_{\mathbf{i}} = \begin{bmatrix}\omega_{\mathbf{i}}z_{2\mathbf{i}}\\ -\omega_{\mathbf{i}}z_{1\mathbf{i}}\\ 0\end{bmatrix} + \begin{bmatrix}u_{1\mathbf{i}}\\ \Psi_{\mathbf{i}}\\ u_{2\mathbf{i}}\end{bmatrix} + \begin{bmatrix}\delta_{x\mathbf{i}}\\ \delta_{y\mathbf{i}}\\ \delta_{\omega\mathbf{i}}\end{bmatrix}. \tag{11}$$

The term $\Psi_{\mathbf{i}}$ in (11) is given in terms of relative orientation and motion of the agent **i** and its neighbors as

$$\begin{aligned}\Psi_{\mathbf{i}} = &\,\omega_{\mathbf{i}}v_{x\mathbf{i}} + s_{(\mathbf{i}-\bar{\mathbf{i}})}\left(\dot{\bar{v}}_{x\mathbf{i}} - \bar{\omega}_{\mathbf{i}}\bar{v}_{y\mathbf{i}}\right) - c_{(\mathbf{i}-\bar{\mathbf{i}})}\left(\dot{\bar{v}}_{y\mathbf{i}} + \bar{\omega}_{\mathbf{i}}\bar{v}_{x\mathbf{i}}\right)\\ &+ \lambda_2[v_{y\mathbf{i}} + s_{(\mathbf{i}-\bar{\mathbf{i}})}\bar{v}_{x\mathbf{i}} - c_{(\mathbf{i}-\bar{\mathbf{i}})}\bar{v}_{y\mathbf{i}}] + f_{y\mathbf{i}}. \qquad (12)\end{aligned}$$

It is noted that the reduced-order error system (11) has two structural properties: 1) the first term in the right-hand side is reminiscent of the skew-symmetric structure, which is commonly seen in the model reference adaptive control systems [21]; 2) the nominal part of (11) is reminiscent of a cascaded system, i.e., $z_{3\mathbf{i}}$-dynamics are decoupled from $(z_{1\mathbf{i}}, z_{2\mathbf{i}})$-dynamics, and $z_{3\mathbf{i}}(t) \to 0$ implies that the interconnected term $\Psi_{\mathbf{i}}(t) \to 0$. These two structural properties are used later in the control design. It follows from (11) that the *formation control problem* is reduced to deigning the new control inputs $(u_{1\mathbf{i}}, u_{2\mathbf{i}})$ that stabilize the reduced-order error dynamics (11) for all vessels $\mathbf{i} = 1, \ldots, N$.

Remark 2: Compared with the vessel model, the error system (11) has only three states that must be stabilized to achieve the desired formation. The control law is distributed since (11) and the feedback transformations (9), (10) do not require the global position measurements and only depend on the relative pose of the **i**th and **j**th agents and their velocities and accelerations in their own body-fixed frames, which can be measured by onboard sensors (e.g., Lidar, camera, gyroscope, speedometer, IMU, etc.)

B. Formation Control Design

The error system (11) is structured such that the orientation error $z_{3\mathbf{i}}$ is decoupled from the positioning errors $(z_{1\mathbf{i}}, z_{2\mathbf{i}})$ and, thus, can be independently controlled. We emphasize that different control laws may be applied to stabilize the error system (11), for instance, passivity-based control. However, because the error system (11) is not in the (lower-triangular) normal form, traditional control methods, such as the first-order sliding mode control or backstepping control, may impose additional strict conditions on the angular velocity (for example, the angular velocity $\omega_{\mathbf{0}}(t)$ in [18] is assumed to be separated from zero). While *any* nonlinear control technique may be applicable under this framework, we choose supertwisting control in this work due to its simplicity and strong robustness, which only requires boundedness of unknown modeling uncertainties and disturbances. More importantly, the supertwisting control takes advantage of the structural properties of the error system (11), and only a mild condition on the angular velocity is needed, as we shall see later.

We choose the supertwisting control laws as

$$\begin{cases} u_{1\mathbf{i}} = -k_{1\mathbf{i}}|z_{1\mathbf{i}}|^{\frac{1}{2}}\,\mathrm{sign}(z_{1\mathbf{i}}) + \xi_{1\mathbf{i}}\\ \dot{\xi}_{1\mathbf{i}} = -k_{2\mathbf{i}}\,\mathrm{sign}(z_{1\mathbf{i}})\end{cases} \tag{13}$$

$$\begin{cases} u_{2\mathbf{i}} = -k_{3\mathbf{i}}|z_{3\mathbf{i}}|^{\frac{1}{2}}\,\mathrm{sign}(z_{3\mathbf{i}}) + \xi_{2\mathbf{i}}\\ \dot{\xi}_{2\mathbf{i}} = -k_{4\mathbf{i}}\,\mathrm{sign}(z_{3\mathbf{i}})\end{cases} \tag{14}$$

where $k_{1\mathbf{i}}$, $k_{2\mathbf{i}}$, $k_{3\mathbf{i}}$, and $k_{4\mathbf{i}}$ are positive control gains. It follows that under control law (13), the closed-loop $(z_{1\mathbf{i}}, z_{2\mathbf{i}})$-dynamics are given by

$$\begin{aligned}\dot{z}_{1\mathbf{i}} &= -k_{1\mathbf{i}}|z_{1\mathbf{i}}|^{\frac{1}{2}}\,\mathrm{sign}(z_{1\mathbf{i}}) + \rho_{1\mathbf{i}} + \omega_{\mathbf{i}}z_{2\mathbf{i}}\\ \dot{\rho}_{1\mathbf{i}} &= -k_{2\mathbf{i}}\,\mathrm{sign}(z_{1\mathbf{i}}) + \dot{\delta}_{x\mathbf{i}}\\ \dot{z}_{2\mathbf{i}} &= -\omega_{\mathbf{i}}z_{1\mathbf{i}} + \Psi_{\mathbf{i}} + \delta_{y\mathbf{i}}\end{aligned} \tag{15}$$

where $\rho_{1\mathbf{i}} := \xi_{1\mathbf{i}} + \delta_{x\mathbf{i}}$. Furthermore, under control law (14), the closed-loop $z_{3\mathbf{i}}$-dynamics are given by

$$\begin{aligned}\dot{z}_{3\mathbf{i}} &= -k_{3\mathbf{i}}|z_{3\mathbf{i}}|^{\frac{1}{2}}\,\mathrm{sign}(z_{3\mathbf{i}}) + \rho_{2\mathbf{i}}\\ \dot{\rho}_{2\mathbf{i}} &= -k_{4\mathbf{i}}\,\mathrm{sign}(z_{3\mathbf{i}}) + \dot{\delta}_{\omega\mathbf{i}}\end{aligned} \tag{16}$$

where $\rho_{2\mathbf{i}} := \xi_{2\mathbf{i}} + \delta_{\omega\mathbf{i}}$. Note that the closed-loop system (15), (16) has a cascade-like structure, i.e., $z_{3\mathbf{i}}$ enters the $(z_{1\mathbf{i}}, z_{2\mathbf{i}})$-dynamics via the interconnection term $\Psi_{\mathbf{i}}$. It is also important to note that the controllers (9), (10), (13), and (14) are completely distributed and independent of global position measurements. The following theorem provides the main result of this section.

Theorem 1 (Formation Control): Consider a network of $N+1$ heterogeneous underactuated surface vessels with the communication graph $\mathcal{G}$, the node dynamics given by (1a), (1b), and the error dynamics given by (11). Assume that the angular velocity of the group leader is persistently exciting (PE), i.e., there exist two constants $T > 0, \mu > 0$ such that $\omega_{\mathbf{0}}(t)$ satisfies

$$\int_t^{t+T} |\omega_{\mathbf{0}}(\tau)|\mathrm{d}\tau \geq \mu \quad \forall t \geq 0.$$

1) Then, without perturbations (i.e., $\delta_{x\mathbf{i}} \equiv \delta_{y\mathbf{i}} \equiv \delta_{\omega\mathbf{i}} \equiv 0$), under the supertwisting control laws (13), (14) with positive gains $k_{1\mathbf{i}}$, $k_{2\mathbf{i}}$, $k_{3\mathbf{i}}$, and $k_{4\mathbf{i}}$, the origin of closed-loop error system (15), (16) is uniformly globally asymptotically stable (UGAS).
2) If the perturbations $\delta_{x\mathbf{i}}(\cdot), \delta_{y\mathbf{i}}(\cdot), \delta_{\omega\mathbf{i}}(\cdot)$ are bounded with bounded derivatives such that (2) holds, and the unmatched uncertainty $\delta_{y\mathbf{i}}(\cdot)$ vanishes with respect to $z_{2\mathbf{i}}$, i.e., $|\delta_{y\mathbf{i}}(\cdot)| \leq \kappa_{\mathbf{i}}|z_{2\mathbf{i}}|$ with $\kappa_{\mathbf{i}} > 0$, then with $k_{2\mathbf{i}} > \Delta_{x\mathbf{i}}$, $k_{4\mathbf{i}} > \Delta_{\omega\mathbf{i}}$, and $k_{1\mathbf{i}}, k_{3\mathbf{i}}$ sufficiently large, the origin of the closed-loop error system (15), (16) is UGAS.

Finally, together with the feedback transformation (9), (10), the *robust formation control problem* is solved.

Proof:

1) Note first that the "upper-left corners" of system (15) (i.e., under $z_{2\mathbf{i}} \equiv 0$) and system (16) are standard supertwisting system. If the control gains $k_{1\mathbf{i}}, k_{2\mathbf{i}}, k_{3\mathbf{i}}, k_{4\mathbf{i}}$ are positive, then the corresponding strict Lyapunov functions can be constructed [22, Th. 1]. That is, for *every* positive definite matrix $Q_{1\mathbf{i}} > 0$ and $Q_{3\mathbf{i}} > 0$, the algebraic Lyapunov equations

$$A_{1\mathbf{i}}^{\top} P_{1\mathbf{i}} + P_{1\mathbf{i}} A_{1\mathbf{i}} = -Q_{1\mathbf{i}},\ A_{3\mathbf{i}}^{\top} P_{3\mathbf{i}} + P_{3\mathbf{i}} A_{3\mathbf{i}} = -Q_{3\mathbf{i}} \tag{17}$$

have unique positive definite solutions $P_{1\mathbf{i}} > 0$ and $P_{3\mathbf{i}} > 0$, where

$$A_{1\mathbf{i}} = \begin{bmatrix} -\frac{1}{2}k_{1\mathbf{i}} & \frac{1}{2} \\ -k_{2\mathbf{i}} & 0 \end{bmatrix},\ A_{3\mathbf{i}} = \begin{bmatrix} -\frac{1}{2}k_{3\mathbf{i}} & \frac{1}{2} \\ -k_{4\mathbf{i}} & 0 \end{bmatrix}.$$

Then, $V_{1\mathbf{i}}(z_{1\mathbf{i}}, \rho_{1\mathbf{i}}) = \zeta_{1\mathbf{i}}^{\top} P_{1\mathbf{i}} \zeta_{1\mathbf{i}}$ and $V_{3\mathbf{i}}(z_{3\mathbf{i}}, \rho_{2\mathbf{i}}) = \zeta_{3\mathbf{i}}^{\top} P_{3\mathbf{i}} \zeta_{3\mathbf{i}}$ are strict Lyapunov functions for system (15) with $z_{2\mathbf{i}} \equiv 0$ and (16), respectively, where $\zeta_{1\mathbf{i}} = [|z_{1\mathbf{i}}|^{1/2}, \rho_{1\mathbf{i}}]^{\top}$ and $\zeta_{3\mathbf{i}} = [|z_{3\mathbf{i}}|^{1/2}, \rho_{2\mathbf{i}}]^{\top}$, and their time derivatives are negative definite

$$\dot{V}_{1\mathbf{i}} = -|z_{1\mathbf{i}}|^{-1/2} \zeta_{1\mathbf{i}}^{\top} Q_{1\mathbf{i}} \zeta_{1\mathbf{i}},\ \dot{V}_{3\mathbf{i}} = -|z_{3\mathbf{i}}|^{-1/2} \zeta_{3\mathbf{i}}^{\top} Q_{3\mathbf{i}} \zeta_{3\mathbf{i}}.$$

Thus, the origin of system (16) is finite-time stable and $z_{3\mathbf{i}}(t)$ reaches zero in finite time. It follows from the definition of $z_{3\mathbf{i}}$ that $(\theta_{\mathbf{i}} - \bar{\theta}_{\mathbf{i}}) \xrightarrow{\exp} 0$ and $(\omega_{\mathbf{i}} - \bar{\omega}_{\mathbf{i}}) \xrightarrow{\exp} 0$ as $t \to \infty$. Then, consider the nominal part of (15), (i.e., (15) with $\Psi_{\mathbf{i}} \equiv 0$). It follows from Lemma 3 in the Appendix that system (15) with $\Psi_{\mathbf{i}} \equiv 0$ is uniformly globally exponentially stable (UGES). Next, it follows from $s_{(\mathbf{i}-\mathbf{j})} \xrightarrow{\exp} 0$ and $c_{(\mathbf{i}-\mathbf{j})} \xrightarrow{\exp} 1$ that (12) reduces to

$$\Psi_{\mathbf{i}} \xrightarrow{\exp} (\dot{v}_{y\mathbf{i}} - \dot{\bar{v}}_{y\mathbf{i}}) + \lambda_2 (v_{y\mathbf{i}} - \bar{v}_{y\mathbf{i}}) + \bar{\omega}_{\mathbf{i}} (v_{x\mathbf{i}} - \bar{v}_{x\mathbf{i}}) \tag{18}$$

and (9) reduces to

$$(\dot{v}_{x\mathbf{i}} - \dot{\bar{v}}_{x\mathbf{i}}) \xrightarrow{\exp} -\lambda_1 (v_{x\mathbf{i}} - \bar{v}_{x\mathbf{i}}) + \bar{\omega}_{\mathbf{i}} (v_{y\mathbf{i}} - \bar{v}_{y\mathbf{i}}). \tag{19}$$

From the model in Section II-B, we have

$$\begin{aligned} (\dot{v}_{y\mathbf{i}} - \dot{\bar{v}}_{y\mathbf{i}}) &= f_{y\mathbf{i}}(v_{x\mathbf{i}}, v_{y\mathbf{i}}, \omega_{\mathbf{i}}) - f_{y\mathbf{i}}(\bar{v}_{x\mathbf{i}}, \bar{v}_{y\mathbf{i}}, \bar{\omega}_{\mathbf{i}}) \\ &= \left[f_{y\mathbf{i}}^{\mathtt{C}}(v_{x\mathbf{i}}, \omega_{\mathbf{i}}) - f_{y\mathbf{i}}^{\mathtt{C}}(\bar{v}_{x\mathbf{i}}, \bar{\omega}_{\mathbf{i}})\right] + \left[f_{y\mathbf{i}}^{\mathtt{D}}(v_{y\mathbf{i}}) - f_{y\mathbf{i}}^{\mathtt{D}}(\bar{v}_{y\mathbf{i}})\right]. \end{aligned} \tag{20}$$

Then, (19) and (20) can be written as

$$\begin{bmatrix} \dot{v}_{x\mathbf{i}} - \dot{\bar{v}}_{x\mathbf{i}} \\ \dot{v}_{y\mathbf{i}} - \dot{\bar{v}}_{y\mathbf{i}} \end{bmatrix} = \begin{bmatrix} -\lambda_1 & \bar{\omega}_{\mathbf{i}}(t) \\ -\eta_{\mathbf{i}} \bar{\omega}_{\mathbf{i}}(t) & \mathcal{D}_{\mathbf{i}}(t) \end{bmatrix} \begin{bmatrix} v_{x\mathbf{i}} - \bar{v}_{x\mathbf{i}} \\ v_{y\mathbf{i}} - \bar{v}_{y\mathbf{i}} \end{bmatrix} + o(t) \tag{21}$$

where $o(\cdot) : \mathbb{R} \to \mathbb{R}^2$ and $|o(t)| \xrightarrow{\exp} 0$; $\mathcal{D}_{\mathbf{i}}(t) := [f_{y\mathbf{i}}^{\mathtt{D}}(v_{y\mathbf{i}}) - f_{y\mathbf{i}}^{\mathtt{D}}(\bar{v}_{y\mathbf{i}})]/[v_{y\mathbf{i}} - \bar{v}_{y\mathbf{i}}]$. It follows from the vessel model in Section II-B that $\mathcal{D}_{\mathbf{i}}(t) \leq 0$ for all $t \geq 0$. Then, from Lemma 3 again, we conclude that the origin of system (21) is UGES, which implies that $\Psi_{\mathbf{i}} \xrightarrow{\exp} 0$. Finally, we conclude that the origin of full dynamics (15), (16) is UGAS using the output injection lemma [23, Proposition 3] by considering that $\Psi_{\mathbf{i}} \in \mathcal{L}_2$ is the uniformly integrable output.

2) If $\delta_{y\mathbf{i}} \equiv 0$ and if the gains $k_{2\mathbf{i}} > \Delta_{x\mathbf{i}}$, $k_{4\mathbf{i}} > \Delta_{\omega\mathbf{i}}$, and $k_{1\mathbf{i}}, k_{3\mathbf{i}}$ are sufficiently large, then it follows from [22, Th. 2] that for *some* positive definite matrices $Q_{1\mathbf{i}} > 0$ and $Q_{3\mathbf{i}} > 0$, the algebraic Lyapunov equations (17) have positive definite solutions $P_{1\mathbf{i}} > 0$ and $P_{3\mathbf{i}} > 0$, and thus, $V_{1\mathbf{i}}$ and $V_{3\mathbf{i}}$ are the strict Lyapunov functions for system (15) with $z_{2\mathbf{i}} \equiv 0$ and (16), respectively. If $\delta_{y\mathbf{i}}(\cdot)$ vanishes with respect to $z_{2\mathbf{i}}$, then it follows from [21, Lemma 9.1] that the origin of the nominal part of the system (15) is UGES if $k_{1\mathbf{i}}$ and $k_{3\mathbf{i}}$ are sufficiently large. Then, the rest of the proof is the same as 1) and the origin of error dynamics (15), (16) is UGAS.

Finally, we conclude that the robust formation control problem is solved from Lemma 1. □

Remark 3: A selection rule for the gains $k_{1\mathbf{i}}, k_{3\mathbf{i}}$ is such that the "upper left corners" of system (15) (i.e., $z_{2\mathbf{i}} \equiv 0$) and system (16) are finite-time stables. The selection rule for sufficiently large control gains $k_{1\mathbf{i}}, k_{3\mathbf{i}}$ is given by [24]

$$k_{1\mathbf{i}} > \sqrt{\frac{2(k_{2\mathbf{i}} + \Delta_{x\mathbf{i}})^2}{k_{2\mathbf{i}} - \Delta_{x\mathbf{i}}}},\ k_{3\mathbf{i}} > \sqrt{\frac{2(k_{4\mathbf{i}} + \Delta_{\omega\mathbf{i}})^2}{k_{4\mathbf{i}} - \Delta_{\omega\mathbf{i}}}}.$$

Remark 4: Although in Theorem 1-2) we assume that unmatched uncertainty $\delta_{y\mathbf{i}}(\cdot)$ vanishes with respect to $z_{2\mathbf{i}}$ to guarantee the *asymptotic stability* of the error system, it should be noted that sea currents and waves are nonvanishing perturbations in practice. Other perturbations $\delta_{x\mathbf{i}}(\cdot)$, $\delta_{\omega\mathbf{i}}(\cdot)$ are assumed to be simply bounded with bounded derivatives since control inputs directly affect surge and yaw motion. In order to stabilize the lateral dynamics, we have to make an assumption about vanishing lateral perturbations due to the fact that the vehicles are underactuated. Note that asymptotic stability is less practical under unknown unmatched disturbances. However, as pointed in [25], in marine practice, the hydrodynamic damping forces in the second equation of (1b) are dominant in the sway direction. As a result, the sway velocity of the surface vessel is passive bounded, and thus, it is uniformly ultimately bounded [26] if $\delta_{y\mathbf{i}}(\cdot)$ is a nonvanishing perturbation. Moreover, as shown in recent works on underactuated systems [27], [28], it is still possible to reject the unknown unmatched perturbations $\delta_{y\mathbf{i}}(\cdot)$ using disturbance observer-based sliding mode control.

IV. Distributed Obstacle Avoidance

A. Elliptical Limit Cycles

Obstacle and collision avoidance is essential in formation control of vehicle networks. In this section, we present a distributed robust obstacle avoidance approach based on the limit cycle design presented in [29]. The method proposed in [29] is to define transient reference trajectories using dynamic systems with elliptical limit cycles. Driven by practical considerations, we assume finite number of obstacles as well as finite number of obstacle encounters. We assume that every obstacle is enclosed by an ellipse, which also serves as a stable limit cycle, and thus, a trajectory starting outside the ellipse will never enter it. Most

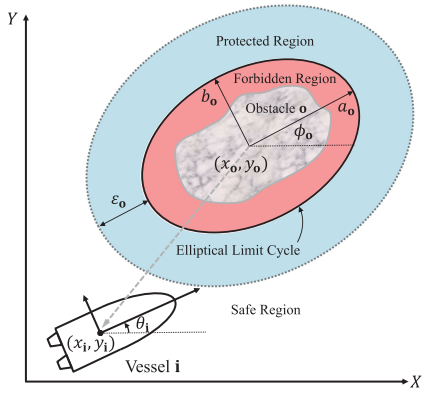

Fig. 2. Top view of the obstacle avoidance of underactuated surface vessels $\mathbf{i}$ and obstacle $\mathbf{o}$.

closed shapes can be efficiently encircled by an ellipse and when two or more obstacles are too close to each other, they can be approximately viewed as a single obstacle enclosed by a larger ellipse.

To illustrate, consider the $\mathbf{i}$th surface vessel in the neighborhood of an arbitrarily-shaped obstacle $\mathbf{o}$ and surrounded by an ellipse marking the *forbidden region* that the vessel must not enter, as shown in Fig. 2. Next, consider the following system that represents planar particle motion whose solution converges to the limit cycle $l_{\mathbf{o}}(t, \chi_1, \chi_2) = 0$:

$$\begin{aligned} \dot{\chi}_1 &= h_1(t, \chi_1, \chi_2) - k_l l_{\mathbf{o}}(t, \chi_1, \chi_2)\chi_1 \\ \dot{\chi}_2 &= h_2(t, \chi_1, \chi_2) - k_l l_{\mathbf{o}}(t, \chi_1, \chi_2)\chi_2 \end{aligned} \tag{22}$$

where $k_l > 0$ is a constant that determines the rate of convergence to the limit cycle. Functions h_1 and h_2 represent the planar particle motion kinematics on the ellipse $l_{\mathbf{o}}(t, \chi_1, \chi_2) = 0$, which are given by

$$\begin{aligned} h_1(t, \chi_1, \chi_2) &= -\chi_2 \dot{\phi}_{\mathbf{o}} + \frac{\varpi_{\mathbf{o}}}{a_{\mathbf{o}} b_{\mathbf{o}}} (h_{11}\chi_1 - h_{12}\chi_2) \\ h_2(t, \chi_1, \chi_2) &= +\chi_1 \dot{\phi}_{\mathbf{o}} + \frac{\varpi_{\mathbf{o}}}{a_{\mathbf{o}} b_{\mathbf{o}}} (h_{21}\chi_1 - h_{11}\chi_2) \end{aligned}$$

where

$$\begin{aligned} h_{11} &:= \left(a_{\mathbf{o}}^2 - b_{\mathbf{o}}^2\right) \sin\phi_{\mathbf{o}} \cos\phi_{\mathbf{o}} \\ h_{12} &:= a_{\mathbf{o}}^2 \cos^2\phi_{\mathbf{o}} + b_{\mathbf{o}}^2 \sin^2\phi_{\mathbf{o}} \\ h_{21} &:= b_{\mathbf{o}}^2 \cos^2\phi_{\mathbf{o}} + a_{\mathbf{o}}^2 \sin^2\phi_{\mathbf{o}} \end{aligned}$$

and $\varpi_{\mathbf{o}}$ is a constant control parameter representing the angular velocity of the particle moving around the ellipse. Note that $\varpi_{\mathbf{o}} > 0$ represents the counterclockwise rotation of the particle, and $\varpi_{\mathbf{o}} < 0$ represents the clockwise rotation of the particle. The following lemma illustrates that the ellipse $l_{\mathbf{o}}(t, \chi_1, \chi_2) = 0$ also serves as a stable limit cycle.

Lemma 2: The periodic solution to planar system (22) on the ellipse $l_{\mathbf{o}}(t, \chi_1, \chi_2) = 0$ given by

$$\begin{aligned} \chi_1(t) &= a_{\mathbf{o}} \cos\phi_{\mathbf{o}} \cos(\varpi_{\mathbf{o}} t) - b_{\mathbf{o}} \sin\phi_{\mathbf{o}} \sin(\varpi_{\mathbf{o}} t) \\ \chi_2(t) &= a_{\mathbf{o}} \sin\phi_{\mathbf{o}} \cos(\varpi_{\mathbf{o}} t) + b_{\mathbf{o}} \cos\phi_{\mathbf{o}} \sin(\varpi_{\mathbf{o}} t) \end{aligned} \tag{23}$$

is asymptotically orbitally stable.

Proof: Taking the time derivative of (23), one can verify that (23) is a solution to (22), and the closed orbit generated by (23) is a positively invariant set. Consider the following Lyapunov candidate function:

$$U(t, x, y) = \frac{1}{4} l_{\mathbf{o}}(t, \chi_1, \chi_2)^2$$

and take its time derivative along the trajectory of (22)

$$\begin{aligned} \dot{U} &= \frac{1}{2} l_{\mathbf{o}}(t, \chi_1, \chi_2)\, \dot{l}_{\mathbf{o}}(t, \chi_1, \chi_2) \\ &= -\frac{k_l}{a_{\mathbf{o}}^2 b_{\mathbf{o}}^2} l_{\mathbf{o}}(t, \chi_1, \chi_2)^2 \left[h_{21}\chi_1^2 + h_{12}\chi_2^2 - 2h_{11}\chi_1\chi_2\right] \\ &= -k_l l_{\mathbf{o}}(t, \chi_1, \chi_2)^2 \left[l_{\mathbf{o}}(t, \chi_1, \chi_2) + 1\right] \le 0. \end{aligned}$$

Thus, for all $(\chi_1, \chi_2) \neq (0, 0)$, $l_{\mathbf{o}}(t, \chi_1, \chi_2) \neq 0$ and all $t \ge 0$, we have $\dot{U} < 0$ since $l_{\mathbf{o}} + 1 > 0$ everywhere on the plane except at the point $(x_{\mathbf{0}}, y_{\mathbf{0}})$ where $\dot{U} = 0$. Thus, from the invariance principle, we conclude that the invariant set $\{(\chi_1, \chi_2) \in \mathbb{R}^2 : l_{\mathbf{o}}(t, \chi_1, \chi_2) = 0\}$ is the asymptotically stable. □

Lemma 2: illustrates that for any initial time t_0, if the initial condition of (22) $(\chi_1(t_0), \chi_2(t_0)) \neq (0, 0)$, that is, $x(t_0) \neq x_{\mathbf{o}}(t_0)$, $y(t_0) \neq y_{\mathbf{o}}(t_0)$, then $l_{\mathbf{o}}(t, \chi_1(t), \chi_2(t))$ is uniformly bounded for all $t \ge t_0$ and converges to zero *asymptotically*. Furthermore, if initial condition is outside the ellipse, i.e., $l_{\mathbf{o}}(t_0, \chi_1(t_0), \chi_2(t_0)) > 0$, then the trajectory of $l_{\mathbf{o}}(t, \chi_1(t), \chi_2(t))$ converges to zero *exponentially*. In this case, for all $t \ge t_0$, we have $l_{\mathbf{o}}(t, \chi_1(t), \chi_2(t)) > 0$, and thus, the trajectory of $(x(t), y(t))$ will never cross the ellipse.

Based on the discussion above, for the $\mathbf{i}$th vessel, if the position trajectory $(x_{\mathbf{i}}(t), y_{\mathbf{i}}(t))$ is a solution to the planar system (22), then its position trajectory is bounded for all times and exponentially converges to the stable elliptical limit cycle generated by the planar system (22). More importantly, the vessel will never cross the limit cycle, which is the foundation of our obstacle avoidance strategy.

B. Obstacle Avoidance Control Design

Similar to the formation control design, in the neighborhood of the obstacle $\mathbf{o}$, the obstacle avoidance error $\zeta_{\mathbf{i}} = (\zeta_{1\mathbf{i}}, \zeta_{2\mathbf{i}})$ for the agent $\mathbf{i}$ is defined using the following transformation:

$$\begin{bmatrix} \zeta_{1\mathbf{i}} \\ \zeta_{2\mathbf{i}} \end{bmatrix} = J_2(\theta_{\mathbf{i}}) \begin{bmatrix} \dot{\tilde{x}}_{\mathbf{io}} - h_1(t, \tilde{x}_{\mathbf{io}}, \tilde{y}_{\mathbf{io}}) + k_l l_{\mathbf{o}}(t, \tilde{x}_{\mathbf{io}}, \tilde{y}_{\mathbf{io}})\tilde{x}_{\mathbf{io}} \\ \dot{\tilde{y}}_{\mathbf{io}} - h_2(t, \tilde{x}_{\mathbf{io}}, \tilde{y}_{\mathbf{io}}) + k_l l_{\mathbf{o}}(t, \tilde{x}_{\mathbf{io}}, \tilde{y}_{\mathbf{io}})\tilde{y}_{\mathbf{io}} \end{bmatrix}$$

where

$$J_2(\theta_{\mathbf{i}}) = \begin{bmatrix} \cos\theta_{\mathbf{i}} & \sin\theta_{\mathbf{i}} \\ -\sin\theta_{\mathbf{i}} & \cos\theta_{\mathbf{i}} \end{bmatrix}.$$

The reason of defining $(\zeta_{1\mathbf{i}}, \zeta_{2\mathbf{i}})$ in this form is that if $(\zeta_{1\mathbf{i}}, \zeta_{2\mathbf{i}}) \equiv (0, 0)$, then $(\tilde{x}_{\mathbf{io}}(t), \tilde{y}_{\mathbf{io}}(t))$ must be a solution of planar system (22), and the position trajectory $(x_{\mathbf{i}}(t), y_{\mathbf{i}}(t))$ exponentially converges to the elliptical limit cycle $l_{\mathbf{o}}(t, \chi_1, \chi_2) = 0$ without crossing it. We calculate the obstacle avoidance error dynamics by taking the time derivative of $\zeta_{\mathbf{i}}$. Under the feedback transformation

$$\tau_{1\mathbf{i}} = -f_{x\mathbf{i}} + \omega_{\mathbf{i}} v_{y\mathbf{i}} - \cos\theta_{\mathbf{i}} \left(k_l \dot{\tilde{x}}_{\mathbf{io}} l_{\mathbf{o}} + k_l \tilde{x}_{\mathbf{io}} \dot{l}_{\mathbf{o}} - \ddot{x}_{\mathbf{o}} - \dot{h}_1\right)$$

$$- \sin\theta_{\mathbf{i}} \left(k_l \dot{\tilde{y}}_{\mathbf{io}} l_{\mathbf{o}} + k_l \tilde{y}_{\mathbf{io}} \dot{l}_{\mathbf{o}} - \ddot{y}_{\mathbf{o}} - \dot{h}_2 \right) + u_{1\mathbf{i}} \tag{24}$$

the obstacle avoidance error dynamics become

$$\begin{bmatrix} \dot{\zeta}_{1\mathbf{i}} \\ \dot{\zeta}_{2\mathbf{i}} \end{bmatrix} = \begin{bmatrix} \omega_{\mathbf{i}} \zeta_{2\mathbf{i}} \\ -\omega_{\mathbf{i}} \zeta_{1\mathbf{i}} \end{bmatrix} + \begin{bmatrix} u_{1\mathbf{i}} \\ \Xi_{\mathbf{i}} \end{bmatrix} + \begin{bmatrix} \delta_{x\mathbf{i}} \\ \delta_{y\mathbf{i}} \end{bmatrix} \tag{25}$$

where

$$\Xi_{\mathbf{i}} := f_{y\mathbf{i}} + \omega_{\mathbf{i}} v_{x\mathbf{i}} - \sin\theta_{\mathbf{i}} \left(k_l \dot{\tilde{x}}_{\mathbf{io}} l_{\mathbf{o}} + k_l \tilde{x}_{\mathbf{io}} \dot{l}_{\mathbf{o}} - \ddot{x}_{\mathbf{o}} - \dot{h}_1 \right) + \cos\theta_{\mathbf{i}} \left(k_l \dot{\tilde{y}}_{\mathbf{io}} l_{\mathbf{o}} + k_l \tilde{y}_{\mathbf{io}} \dot{l}_{\mathbf{o}} - \ddot{y}_{\mathbf{o}} - \dot{h}_2 \right).$$

Compared to the reduced-order error system (11), the error system (25) has a similar structure property, that is, the first term in the right-hand side is reminiscent of the skew-symmetric structure. Thus, we choose a similar supertwisting control law as

$$\begin{cases} u_{1\mathbf{i}} = -k_{1\mathbf{i}} |\zeta_{1\mathbf{i}}|^{\frac{1}{2}} \operatorname{sign}(\zeta_{1\mathbf{i}}) + \xi_{1\mathbf{i}} \\ \dot{\xi}_{1\mathbf{i}} = -k_{2\mathbf{i}} \operatorname{sign}(\zeta_{1\mathbf{i}}) \end{cases} \tag{26}$$

where $k_{1\mathbf{i}}, k_{2\mathbf{i}}$ are positive control gains. Furthermore, if $v_{x\mathbf{i}} \neq 0$, then $\Xi_{\mathbf{i}}$ can be controlled by viewing $\omega_{\mathbf{i}}$ as a virtual control input and using backstepping procedure to obtain $\tau_{2\mathbf{i}}$. The virtual control is chosen as

$$\hat{\omega}_{\mathbf{i}} = -\frac{1}{v_{x\mathbf{i}}} \left[f_{y\mathbf{i}} - \sin\theta_{\mathbf{i}} \left(k_l \dot{\tilde{x}}_{\mathbf{io}} l_{\mathbf{o}} + k_l \tilde{x}_{\mathbf{io}} \dot{l}_{\mathbf{o}} - \ddot{x}_{\mathbf{o}} - \dot{h}_1 \right) + \cos\theta_{\mathbf{i}} \left(k_l \dot{\tilde{y}}_{\mathbf{io}} l_{\mathbf{o}} + k_l \tilde{y}_{\mathbf{io}} \dot{l}_{\mathbf{o}} - \ddot{y}_{\mathbf{o}} - \dot{h}_2 \right) \right]$$

and the super-twisting control $\tau_{2\mathbf{i}}$ is designed as

$$\begin{cases} \tau_{2\mathbf{i}} = -f_{\omega\mathbf{i}} + \dot{\hat{\omega}}_{\mathbf{i}} - k_{3\mathbf{i}} |\tilde{\omega}_{\mathbf{i}}|^{\frac{1}{2}} \operatorname{sign}(\tilde{\omega}_{\mathbf{i}}) + \xi_{2\mathbf{i}} \\ \dot{\xi}_{2\mathbf{i}} = -k_{4\mathbf{i}} \operatorname{sign}(\tilde{\omega}_{\mathbf{i}}) \end{cases} \tag{27}$$

where $k_{3\mathbf{i}}$, $k_{4\mathbf{i}}$ are positive control gains, and $\tilde{\omega}_{\mathbf{i}} := \omega_{\mathbf{i}} - \hat{\omega}_{\mathbf{i}}$. Then, under the control law (26), the closed-loop system of $(\zeta_{1\mathbf{i}}, \zeta_{2\mathbf{i}})$-dynamics become

$$\begin{aligned} \dot{\zeta}_{1\mathbf{i}} &= -k_{1\mathbf{i}} |\zeta_{1\mathbf{i}}|^{\frac{1}{2}} \operatorname{sign}(\zeta_{1\mathbf{i}}) + \rho_{1\mathbf{i}} + \omega_{\mathbf{i}} \zeta_{2\mathbf{i}} \\ \dot{\rho}_{1\mathbf{i}} &= -k_{2\mathbf{i}} \operatorname{sign}(\zeta_{1\mathbf{i}}) + \dot{\delta}_{x\mathbf{i}} \\ \dot{\zeta}_{2\mathbf{i}} &= -\omega_{\mathbf{i}} \zeta_{1\mathbf{i}} + \Xi_{\mathbf{i}} + \delta_{y\mathbf{i}} \end{aligned} \tag{28}$$

where $\rho_{1\mathbf{i}} := \xi_{1\mathbf{i}} + \delta_{x\mathbf{i}}$, and under control law (27), the closed-loop system of $\tilde{\omega}_{\mathbf{i}}$-dynamics become

$$\begin{aligned} \dot{\tilde{\omega}}_{\mathbf{i}} &= -k_{3\mathbf{i}} |\tilde{\omega}_{\mathbf{i}}|^{\frac{1}{2}} \operatorname{sign}(\tilde{\omega}_{\mathbf{i}}) + \rho_{2\mathbf{i}} \\ \dot{\rho}_{2\mathbf{i}} &= -k_{4\mathbf{i}} \operatorname{sign}(\tilde{\omega}_{\mathbf{i}}) + \dot{\delta}_{\omega\mathbf{i}}. \end{aligned} \tag{29}$$

We emphasis that the obstacle avoidance controllers given in (24), (26) and (27) are completely independent of global position measurements of both the vessel and obstacle. The next theorem provides the main result of this section.

Theorem 2 (Obstacle Avoidance): Let the surface vessel $\mathbf{i}$ given by (1a) and (1b) be in the neighborhood of an obstacle $\mathbf{o}$ with the obstacle avoidance error dynamics given by (25). Assume that $v_{x\mathbf{i}} \neq 0$, and the angular velocity of the vessel is PE, i.e., there exist two constants $T > 0, \mu > 0$ such that $\omega_{\mathbf{i}}(\cdot)$ satisfies

$$\int_t^{t+T} |\omega_{\mathbf{i}}(\tau)| \mathrm{d}\tau \geq \mu \quad \forall t \geq 0.$$

1) Then, without perturbations, i.e., $\delta_{x\mathbf{i}} \equiv \delta_{y\mathbf{i}} \equiv \delta_{\omega\mathbf{i}} \equiv 0$, under the supertwisting control laws (26), (27) with positive control gains $k_{1\mathbf{i}}$, $k_{2\mathbf{i}}$, $k_{3\mathbf{i}}$, and $k_{4\mathbf{i}}$, the origin of the closed-loop system (28), (29) is UGES.
2) If the perturbations $\delta_{x\mathbf{i}}(\cdot), \delta_{y\mathbf{i}}(\cdot), \delta_{\omega\mathbf{i}}(\cdot)$ are bounded with bounded derivatives satisfying (2), and $\delta_{y\mathbf{i}}(\cdot)$ vanishes with respect to $z_{2\mathbf{i}}$, i.e., $|\delta_{y\mathbf{i}}(\cdot)| \leq \kappa_{\mathbf{i}} |z_{2\mathbf{i}}|$ with $\kappa_{\mathbf{i}} > 0$, then, with $k_{2\mathbf{i}} > \Delta_{x\mathbf{i}}, k_{4\mathbf{i}} > \Delta_{\omega\mathbf{i}}$, and $k_{1\mathbf{i}}, k_{3\mathbf{i}}$ sufficiently large, the origin of the closed-loop system (15), (16) is UGES.

Finally, together with the feedback transformation (24), the *distributed obstacle avoidance problem* is solved.

Proof: The proof is closely parallel to that of *Theorem 1*.

1) Similar to the proof of Theorem 1, the "upper-left corners" of system (28) (i.e., under $\zeta_{2\mathbf{i}} \equiv 0$) and system (29) are standard supertwisting systems. It follows from [22] that if the control gains $k_{1\mathbf{i}}$, $k_{2\mathbf{i}}$, $k_{3\mathbf{i}}$, $k_{4\mathbf{i}}$ are positive, then the system (28) with $\zeta_{2\mathbf{i}} \equiv 0$ and system (29) are finite-time stable. Thus, $\tilde{\omega}_{\mathbf{i}}$ reaches zero in a finite time, which implies that $\omega_{\mathbf{i}} = \hat{\omega}_{\mathbf{i}}$ and $\Xi_{\mathbf{i}} = 0$ after some finite time T. Next, note that the finite-time stability of the "upper-left corner" of (28) also implies exponential stability. Then, from Lemma 3 and the PE assumption of $\omega_{\mathbf{i}}(\cdot)$, we conclude that the nominal part of system (28) is UGES. Finally, it follows from the output injection lemma [23, Proposition 4] that the origin of the full dynamics (28), (29) is UGES by noting that $\Xi_{\mathbf{i}}$ is the uniformly integrable output.
2) If $\delta_{y\mathbf{i}} \equiv 0$ and if the control gains $k_{2\mathbf{i}} > \Delta_{x\mathbf{i}}, k_{4\mathbf{i}} > \Delta_{\omega\mathbf{i}}$, and $k_{1\mathbf{i}}, k_{3\mathbf{i}}$ are sufficiently large, then it follows from [22] that the system (28) with $\zeta_{2\mathbf{i}} \equiv 0$ and system (29) are finite-time stable. If $\delta_{y\mathbf{i}}(\cdot)$ satisfies the vanishing perturbation condition with respect to $z_{2\mathbf{i}}$, then it follows from [21, Lemma 9.1] that the origin of the nominal part of the system (15) is UGES if $k_{1\mathbf{i}}$ and $k_{3\mathbf{i}}$ are sufficiently large. Then the rest of the proof is the same as 1) and the origin of the closed-loop error systems (15), (16) is UGES. Finally, together with Lemma 2, we conclude that the distributed obstacle avoidance problem is solved.

Remark 5: From the proof of Lemma 2, the convergence rate of $l_{\mathbf{o}}(t, \tilde{x}_{\mathbf{io}}, \tilde{y}_{\mathbf{io}})$ is determined by the control parameter k_l and can be estimated using the Lyapunov function $U(t, x_{\mathbf{i}}, y_{\mathbf{i}})$. Furthermore, the error $\zeta_{\mathbf{i}} \to 0$ implies that the position trajectory $(x_{\mathbf{i}}(t), y_{\mathbf{i}}(t))$ converges to a solution to the planar system (22). By designing the appropriate convergence speed of $\zeta_{\mathbf{i}}$, one can guarantee that $(x_{\mathbf{i}}(t), y_{\mathbf{i}}(t))$ converges to the elliptical limit cycle without crossing it.

C. Distributed Obstacle Avoidance Algorithm

Consider a network of $N+1$ heterogeneous underactuated surface vessels in coordinated motion with the controller given in Theorem 1. Assume that the approximate sizes and locations of obstacles in the vicinity of any surface vessel can be measured

by its onboard sensors, e.g., camera, Lidar, etc. The strategy for obstacle avoidance in the coordinated motion of surface vessel networks is described as follows.

Step 1: All obstacles including other vessels in the vicinity of the **i**th vessel are identified and indexed as $\mathbf{o} \in \{1, 2, \ldots, M\} =: \mathcal{O}$. The obstacles are approximated and enclosed by ellipses based on their sizes, orientations, and locations. The inner regions of the ellipses $\mathcal{Q}_\mathbf{o} := \{(x, y) : l_\mathbf{o}(t, \tilde{x}_\mathbf{io}, \tilde{y}_\mathbf{io}) < 0\}$ are prohibited, i.e., vessels are *forbidden* to enter these regions.

Step 2: Define a *protected region* $\mathcal{P}_\mathbf{o}$ for any ellipse such that $\mathcal{P}_\mathbf{o} := \{(x, y) : \text{dist}\{(x, y), \mathcal{Q}_\mathbf{o}\} \le \varepsilon_\mathbf{o},\ l_\mathbf{o}(t, \tilde{x}_\mathbf{io}, \tilde{y}_\mathbf{io}) \ge 0\}$, where $\varepsilon_\mathbf{o} > 0$ is a constant, and $\text{dist}\{(x, y), \mathcal{Q}_\mathbf{o}\} = \inf_{(p,q)\in\mathcal{Q}_\mathbf{o}} |(x, y) - (p, q)|$. Then, the safe region of obstacle $\mathbf{o}$ is defined as $\mathcal{S}_\mathbf{o} := \mathbb{R}^2 \setminus \{\mathcal{P}_\mathbf{o} \cup \mathcal{Q}_\mathbf{o}\}$, as shown in Fig. 2. We also assume that $\mathcal{P}_{\mathbf{o_1}} \cap \mathcal{P}_{\mathbf{o_2}} = \varnothing$, for any $\mathbf{o_1}, \mathbf{o_2} \in \mathcal{O}$, and all the vessels are in the safe regions at the initial time.

Step 3: If the **i**th vessel is in the protected region of the **o**th obstacle and if the direction of its velocity vector relative to the obstacle is toward $\mathcal{Q}_\mathbf{o}$ (i.e., vessel is on a collision course with the obstacle), then the control strategy switches from the formation control strategy given in Theorem 1 to the obstacle avoidance control strategy given in Theorem 2. Note that if the **i**th vessel is in the obstacle avoidance phase, its trajectory exponentially converges to the elliptical orbit, and by selecting the control gains $\min\{k_{1\mathbf{i}}, k_{3\mathbf{i}}\} > k_l$, its trajectory will never cross the ellipse.

Step 4: As soon as the obstacle is cleared, that is, the ellipse is not blocking the agent's direct path to its current desired position $(\bar{x}_\mathbf{i}, \bar{y}_\mathbf{i})$, vessel **i** switches back to its formation tracking control strategy given in Theorem 1.

Step 5: The **i**th vessel continues executing the formation task. If a new obstacle is detected, then *Steps 1–4* are repeated.

Remark 6: Note that for each vessel, switching into obstacle avoidance mode occurs if it enters the protected region surrounding an obstacle and its relative velocity vector points toward the obstacle. The limit cycle solution guarantees that the vessel will go around the obstacle and at some point its relative velocity will not be pointing toward the obstacle. In other words, the obstacle is cleared and the vessels exit obstacle avoidance mode. If several obstacles are tightly located, they can be enclosed by a single larger ellipse. Based on practical considerations, we assume the finite number of obstacles as well as obstacle encounters, and once all obstacles are cleared, the control strategy switches back to formation control strategy (13), (14) whose stability is proven in Theorem 1.

V. Vessel Models

Vessels are normally modeled with either diagonal or coupled mass matrices and either linear or nonlinear hydrodynamic damping. Our framework can be applied to any of these models. In the simplest and most common form, when the **i**th vessel is modeled with diagonal mass matrix and linear hydrodynamic damping [8], the known terms in (1b) based on nominal parameters are given as

$$f_{x\mathbf{i}} = \frac{m_{22,\mathbf{i}}}{m_{11,\mathbf{i}}} v_{y\mathbf{i}}\omega_\mathbf{i} - \frac{d_{11,\mathbf{i}}}{m_{11,\mathbf{i}}} v_{x\mathbf{i}}$$

$$f_{y\mathbf{i}} = -\frac{m_{11,\mathbf{i}}}{m_{22,\mathbf{i}}} v_{x\mathbf{i}}\omega_\mathbf{i} - \frac{d_{22,\mathbf{i}}}{m_{22,\mathbf{i}}} v_{y\mathbf{i}}$$

$$f_{\omega\mathbf{i}} = \frac{m_{11,\mathbf{i}} - m_{22,\mathbf{i}}}{m_{33,\mathbf{i}}} v_{x\mathbf{i}} v_{y\mathbf{i}} - \frac{d_{33,\mathbf{i}}}{m_{33,\mathbf{i}}} \omega_\mathbf{i} \tag{30}$$

where $m_{11,\mathbf{i}}$ and $m_{22,\mathbf{i}}$ represent the vessel mass including added mass effect and $m_{33,\mathbf{i}}$ is the mass moment of inertia again including the added mass effect. The terms $d_{11,\mathbf{i}}, d_{22,\mathbf{i}}, d_{33,\mathbf{i}}$ represent the hydrodynamic damping coefficients. If vessel **i** is modeled with diagonal mass matrix and nonlinear hydrodynamic damping, as in [30], then the known terms in (1b) take the form

$$f_{x\mathbf{i}} = \frac{m_{22,\mathbf{i}}}{m_{11,\mathbf{i}}} v_{y\mathbf{i}}\omega_\mathbf{i} - \frac{d_{11,\mathbf{i}}}{m_{11,\mathbf{i}}} |v_{x\mathbf{i}}|^{\alpha_{11,\mathbf{i}}} \text{sign}\,(v_{x\mathbf{i}})$$

$$f_{y\mathbf{i}} = -\frac{m_{11,\mathbf{i}}}{m_{22,\mathbf{i}}} v_{x\mathbf{i}}\omega_\mathbf{i} - \frac{d_{22,\mathbf{i}}}{m_{22,\mathbf{i}}} |v_{y\mathbf{i}}|^{\alpha_{22,\mathbf{i}}} \text{sign}\,(v_{y\mathbf{i}})$$

$$f_{\omega\mathbf{i}} = \frac{m_{11,\mathbf{i}} - m_{22,\mathbf{i}}}{m_{33,\mathbf{i}}} v_{x\mathbf{i}} v_{y\mathbf{i}} - \frac{d_{33,\mathbf{i}}}{m_{33,\mathbf{i}}} |\omega_\mathbf{i}|^{\alpha_{33,\mathbf{i}}} \text{sign}\,(\omega_\mathbf{i}) \tag{31}$$

where $\alpha_{11,\mathbf{i}}, \alpha_{22,\mathbf{i}}$, and $\alpha_{33,\mathbf{i}}$ are used for power law representation of hydrodynamic damping.

In practice, a model that includes coupling terms in the mass and hydrodynamic damping matrices may be more realistic. The nominal model in this case is given as in [30]

$$\begin{bmatrix} m_{11,\mathbf{i}} & 0 & 0 \\ 0 & m_{22,\mathbf{i}} & m_{23,\mathbf{i}} \\ 0 & m_{23,\mathbf{i}} & m_{33,\mathbf{i}} \end{bmatrix} \begin{bmatrix} \dot{v}_{x\mathbf{i}} \\ \dot{v}_{y\mathbf{i}} \\ \dot{\omega}_\mathbf{i} \end{bmatrix} + \begin{bmatrix} -m_{22,\mathbf{i}} v_{y\mathbf{i}}\omega_\mathbf{i} - m_{23,\mathbf{i}}\omega_\mathbf{i}^2 \\ m_{11,\mathbf{i}} v_{x\mathbf{i}}\omega_\mathbf{i} \\ -m_{d,\mathbf{i}} v_{x\mathbf{i}} v_{y\mathbf{i}} + m_{23,\mathbf{i}} v_{x\mathbf{i}}\omega_\mathbf{i} \end{bmatrix}$$

$$+ \begin{bmatrix} d_{11,\mathbf{i}} & 0 & 0 \\ 0 & d_{22,\mathbf{i}} & d_{23,\mathbf{i}} \\ 0 & d_{23,\mathbf{i}} & d_{33,\mathbf{i}} \end{bmatrix} \begin{bmatrix} v_{x\mathbf{i}} \\ v_{y\mathbf{i}} \\ \omega_\mathbf{i} \end{bmatrix} = \begin{bmatrix} F_\mathbf{i} \\ 0 \\ T_\mathbf{i} \end{bmatrix}$$

where the parameters $m_{23,\mathbf{i}}$ and $d_{23,\mathbf{i}}$ are nonnegative. These equations may be rewritten in the form of (1b) with the terms

$$f_{x\mathbf{i}} = \frac{m_{22,\mathbf{i}}}{m_{11,\mathbf{i}}} v_{y\mathbf{i}}\omega_\mathbf{i} + \frac{m_{23,\mathbf{i}}}{m_{11,\mathbf{i}}}\omega_\mathbf{i}^2 - \frac{d_{11,\mathbf{i}}}{m_{11,\mathbf{i}}} v_{x\mathbf{i}}$$

$$f_{y\mathbf{i}} = a_{\omega\mathbf{i}} \left(f'_{y\mathbf{i}} - \frac{m_{23,\mathbf{i}}}{m_{22,\mathbf{i}}} f'_{\omega\mathbf{i}} \right), \quad \tau_{1\mathbf{i}} = \frac{F_\mathbf{i}}{m_{11,\mathbf{i}}}$$

$$f_{\omega\mathbf{i}} = a_{\omega\mathbf{i}} \left(f'_{\omega\mathbf{i}} - \frac{m_{23,\mathbf{i}}}{m_{33,\mathbf{i}}} f'_{y\mathbf{i}} \right), \quad \tau_{2\mathbf{i}} = \frac{T_\mathbf{i}}{m_{33,\mathbf{i}}} \tag{32}$$

where

$$f'_{y\mathbf{i}} = -\frac{m_{11,\mathbf{i}}}{m_{22,\mathbf{i}}} v_{x\mathbf{i}}\omega_\mathbf{i} - \frac{d_{22,\mathbf{i}}}{m_{22,\mathbf{i}}} v_{y\mathbf{i}} - \frac{d_{23,\mathbf{i}}}{m_{22,\mathbf{i}}}\omega_\mathbf{i}$$

$$f'_{\omega\mathbf{i}} = \frac{m_{d,\mathbf{i}}}{m_{33,\mathbf{i}}} v_{x\mathbf{i}} v_{y\mathbf{i}} - \frac{m_{23,\mathbf{i}}}{m_{33,\mathbf{i}}} v_{x\mathbf{i}}\omega_\mathbf{i} - \frac{d_{23,\mathbf{i}}}{m_{33,\mathbf{i}}} v_{y\mathbf{i}} - \frac{d_{33,\mathbf{i}}}{m_{33,\mathbf{i}}}\omega_\mathbf{i}$$

$$a_{\omega\mathbf{i}} = \frac{m_{22,\mathbf{i}} m_{33,\mathbf{i}}}{m_{22,\mathbf{i}} m_{33,\mathbf{i}} - m_{23,\mathbf{i}}^2}.$$

VI. Simulation Results

We simulated two heterogeneous surface vessel networks to validate the performance of the proposed robust formation control and distributed obstacle avoidance algorithm. All the parameters are given in SI units.

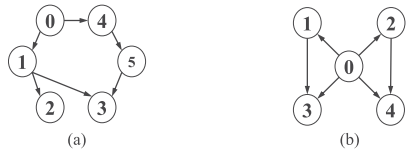

Fig. 3. Directed-tree topology for (a) Example 1 and (b) Example 2.

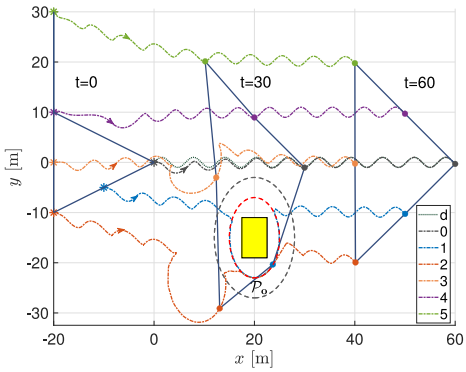

Fig. 4. Paths of the six heterogeneous surface vessels in Example 1 where "d" indicates the leader's desired trajectory.

Example 1: Consider a network of six heterogeneous underactuated surface vessels with the directed communication graph shown in Fig. 3(a), where $w_{\mathbf{31}} = 0.5$, $w_{\mathbf{35}} = 0.5$ and all other weighting coefficients are set to 1. The desired formation shape of the group of vessels is an isosceles right triangle with the leader vessel $\mathbf{0}$ located at the triangle's apex. Vessels $\mathbf{4}$ and $\mathbf{2}$ are located at the other two vertices, vessels $\mathbf{1}$ and $\mathbf{4}$ are located at the midpoints of the two equal sides, and vessel $\mathbf{3}$ is located at the midpoint of the base. The base and the height of the triangle are set to 40 m and 20 m, respectively. In the simulation, the leader is commanded to follow a sinusoidal path, i.e., $(x_{\mathbf{0d}}(t), y_{\mathbf{0d}}(t)) = (t, \sin(t))$.

We assume that vessels $\mathbf{0}, \mathbf{1}$ are modeled by diagonal mass matrix and linear hydrodynamic damping model (30), vessels $\mathbf{2}, \mathbf{3}$ are modeled by the nonlinear hydrodynamic damping model (31), and vessels $\mathbf{4}, \mathbf{5}$ are modeled by the nondiagonal mass and hydrodynamic damping matrices. The model parameters of vessels $\mathbf{0}, \mathbf{1}$ are given as [31] $m_{11,\mathbf{i}} = 1.412, m_{22,\mathbf{i}} = 1.982, m_{33,\mathbf{i}} = 0.0354, d_{11,\mathbf{i}} = 3.436, d_{22,\mathbf{i}} = 12.99, d_{33,\mathbf{i}} = 0.0864$. The model parameters of vessels $\mathbf{2}, \mathbf{3}$ are given as $m_{11,\mathbf{i}} = 1.317, m_{22,\mathbf{i}} = 3.832, m_{33,\mathbf{i}} = 0.0926, d_{11,\mathbf{i}} = 5.252, d_{22,\mathbf{i}} = 14.14, d_{33,\mathbf{i}} = 0.0262, \alpha_{11,\mathbf{i}} = 1.510, \alpha_{22,\mathbf{i}} = 1.747, \alpha_{33,\mathbf{i}} = 1.592$. The model parameters of vessels $\mathbf{4}, \mathbf{5}$ are given as $m_{11,\mathbf{i}} = 1.695, m_{22,\mathbf{i}} = 1.865, m_{33,\mathbf{i}} = 0.0275, d_{11,\mathbf{i}} = 2.72, d_{22,\mathbf{i}} = 13.4, d_{33,\mathbf{i}} = 0.0566, m_{23,\mathbf{i}} = 0.02, d_{23,\mathbf{i}} = -0.03$. All vessels start from rest at the initial positions shown in Fig. 4 and orientation angles being 0 for vessels $\mathbf{0}, \mathbf{1}, \mathbf{2}$ and $\pi/2$ for vessels $\mathbf{3}, \mathbf{4}, \mathbf{5}$. To demonstrate robustness, we assume that the unknown terms $\delta_{x\mathbf{i}}, \delta_{y\mathbf{i}}, \delta_{\omega\mathbf{i}}$ consist of two parts, i.e., bounded disturbances and modeling uncertainties. We apply disturbances $\delta'_{x\mathbf{i}}(t) = \delta'_{\omega\mathbf{i}}(t) = 1 + 0.5\sin(t) + 0.5\sin(20t)$. Furthermore, we assume that the nominal model parameters used in the controllers contain $\pm 10\%$ errors representing the model uncertainties. We also use ODE-based transitional trajectories in the simulation in order to avoid the undesired nonsmooth motion caused by large errors in the beginning of the motion and switching of controllers [29].

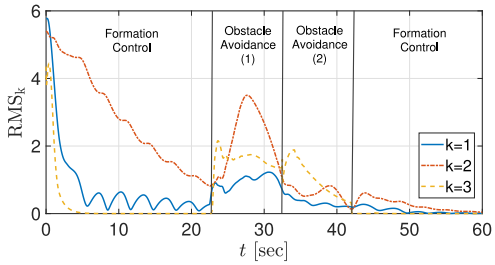

Fig. 5. Time history of the RMS of the three error states combined for all vessels in Example 1.

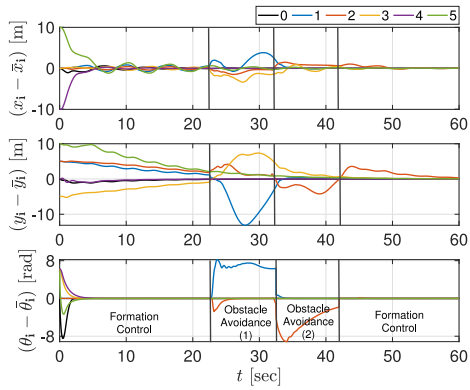

Fig. 6. Time history of the configuration errors of the six surface vessels in Example 1.

The control gains and disturbance bounds are selected as $\lambda_1 = \lambda_2 = \lambda_3 = 1, k_{1\mathbf{i}} = k_{2\mathbf{i}} = k_{3\mathbf{i}} = k_{4\mathbf{i}} = 5, \Delta_{x\mathbf{i}} = 4, \Delta_{y\mathbf{i}} = 3, \Delta_{\omega\mathbf{i}} = 4$, for $\mathbf{i} = 0, \ldots, 5$. To validate the obstacle avoidance algorithm, we assume that a static obstacle $\mathbf{o}$ is located on the desired path of the vessel $\mathbf{1}$, where $(x_{\mathbf{o}}, y_{\mathbf{o}}) = (20, -15)$, and the other parameters of the obstacle and control gains from Theorem 2 are $a_{\mathbf{o}} = 4, b_{\mathbf{o}} = 2.5, \phi_{\mathbf{o}} = \pi/2, \varepsilon_{\mathbf{o}} = 4, \varpi_{\mathbf{o}} = 0.2, k_l = 5, k_{1\mathbf{1}} = k_{2\mathbf{1}} = k_{4\mathbf{1}} = 4, k_{3\mathbf{1}} = 10$.

Simulation results are illustrated in Figs. 4– 6. Fig. 4 shows the paths of all six surface vessels with the formations illustrated at $t = 0$ s, 30 s, and 60 s. Fig. 5 shows the time history of the root-mean squared (RMS) of the error states $z_{1\mathrm{i}}, z_{2\mathrm{i}}$ and $z_{3\mathrm{i}}$ across the formation, i.e.,

$$\mathrm{RMS}_k = \sqrt{\frac{1}{6}\sum_{\mathrm{i}=0}^{5}(z_{k\mathbf{i}})^2}, \ k = 1, 2, 3.$$

The corresponding actual configuration error trajectories for the six heterogeneous vessels are shown in Fig. 6.

In this simulation, the desired triangular formation is initially achieved in approximately 22 s, as indicated by the convergence of RMS values and the configuration errors of all six vessels in Figs. 5 and 6. Then, vessel $\mathbf{1}$ enters the protected region $\mathcal{P}_{\mathbf{o}}$ and switches to the obstacle avoidance mode. In the protected region $\mathcal{P}_{\mathbf{o}}$, the trajectory of vessel $\mathbf{1}$ asymptotically converges to

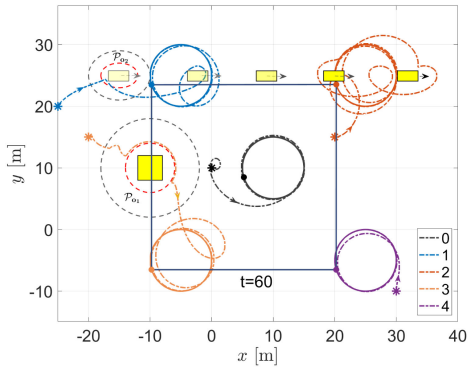

Fig. 7. Paths of the five heterogeneous surface vessels in Example 2.

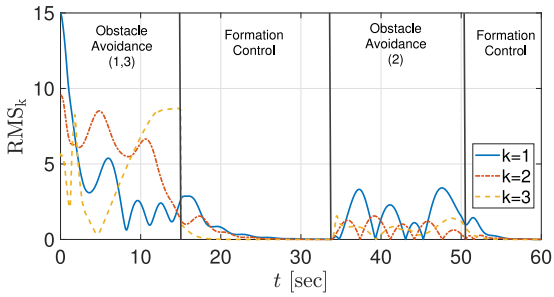

Fig. 8. Time history of the RMS of the three error states combined for all vessels in Example 2.

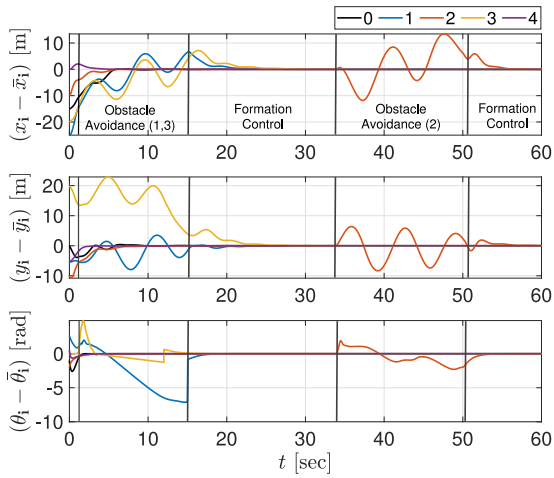

Fig. 9. Time history the configuration errors of the five surface vessels in Example 2.

the predefined elliptical limit cycle without crossing it. When the reference trajectory of vessel $\mathbf{1}$ leaves the forbidden region $\mathcal{Q}_{\mathbf{o}}$, the vessel ignores the obstacle and switches to formation control mode. Note that while vessel $\mathbf{1}$ is in obstacle avoidance mode, vessel $\mathbf{2}$ keeps its formation position relative to $\mathbf{1}$, and vessel $\mathbf{3}$ continues to keep its formation position relative to both vessels $\mathbf{1}$ and $\mathbf{5}$. Thus, the formation geometry deforms to allow obstacle avoidance by $\mathbf{1}$. Next, vessel $\mathbf{2}$ enters the protected region $\mathcal{P}_{\mathbf{o}}$ and switches to the obstacle avoidance mode. After the obstacle is cleared by this vessel at approximately 42 s, it switches back to formation mode. In this case, the motion of no other vessel is affected since vessel $\mathbf{2}$ has no followers. Finally, the desired formation is achieved after approximately 50 s.

Example 2: Consider a network of five heterogeneous underactuated surface vessels with the connected communication graph shown in Fig. 3(b), where the weighting coefficients are set to $w_{\mathbf{10}} = 1, w_{\mathbf{20}} = 1, w_{\mathbf{30}} = 0.5, w_{\mathbf{31}} = 0.5, w_{\mathbf{40}} = 0.8$, and $w_{\mathbf{42}} = 0.2$. The desired formation shape of the four follower vessels is a square with the leader vessel $\mathbf{0}$ located at its center. The length of the square sides is 30 m. In the simulation, the leader is commanded to follow a circle of radius 5 m centered at (10,10) and at a constant speed of 1 rad/s. The models and parameters of vessels $\mathbf{0}$–$\mathbf{4}$ are the same as those given in Example 1. All vessels start from rest at initial positions shown in Fig. 7 . Initial orientation angles are given as $\theta_{\mathbf{0}}(0) = \theta_{\mathbf{2}}(0) = \theta_{\mathbf{3}}(0) = 0$ and $\theta_{\mathbf{1}}(0) = \theta_{\mathbf{4}}(0) = \pi/2$.

The disturbance terms and nominal model parameters are selected the same as in Example 1, and the formation control gains are selected as $\lambda_1 = \lambda_2 = \lambda_3 = 1$ and $k_{1\mathbf{i}} = k_{2\mathbf{i}} = k_{3\mathbf{i}} = k_{4\mathbf{i}} = 6$, for $\mathbf{i} = 0, \ldots, 4$. To validate the obstacle avoidance algorithm, we assume that a static obstacle $\mathbf{o_1}$ and a dynamic obstacle $\mathbf{o_2}$ are located at the paths of the vessels. The parameters of the obstacles and control gains in Theorem 2 are given by $(x_{\mathbf{o_1}}, y_{\mathbf{o_1}}) = (-10, 10), (x_{\mathbf{o_2}}, y_{\mathbf{o_2}}) = (-15 + t, 25), a_{\mathbf{o_1}} = 4, b_{\mathbf{o_1}} = 4, \varphi_{\mathbf{o_1}} = 0, a_{\mathbf{o_2}} = 4, b_{\mathbf{o_2}} = 2, \varphi_{\mathbf{o_2}} = 0, k_{l\mathbf{1}} = 4, \varepsilon_{\mathbf{o_1}} = 4, r_{\mathbf{o_1}} = -0.5, k_{l\mathbf{2}} = 1, \varepsilon_{\mathbf{o_2}} = 2, r_{\mathbf{o_2}} = 0.5, k_{1\mathbf{i}} = k_{2\mathbf{i}} = k_{4\mathbf{i}} = 6, k_{3\mathbf{i}} = 10, \mathbf{i} = 1, 2, 3$.

The simulation results are presented in Figs. 7–9. Fig. 7 shows the paths of the five surface vessels avoiding the obstacles and finally reaching the desired rectangular formation in approximately 60 s. Fig. 8 shows the time history of the RMS of the three error states combined for the five follower vessels, while the time history of the configuration error for the five heterogeneous vessels is shown in Fig. 9. These figures demonstrate that the error dynamics and formation errors are initially stabilized in approximately 30 s and then again after 60 s when all obstacles are cleared.

In the simulation, after only a few seconds, vessels $\mathbf{1}$ and $\mathbf{3}$ almost simultaneously enter the protected regions $\mathcal{P}_{\mathbf{o_2}}$ and $\mathcal{P}_{\mathbf{o_1}}$, respectively, and switch to the obstacle avoidance mode. In the protected region $\mathcal{P}_{\mathbf{o_1}}$, vessel $\mathbf{3}$ asymptotically converges to the elliptical limit cycle without crossing it. Obstacle $\mathbf{o_2}$ is dynamic, and consequently, vessel $\mathbf{1}$ asymptotically converges to the time-varying elliptical limit cycle without crossing it. After detecting that the obstacles are cleared, vessels $\mathbf{1}$ and $\mathbf{3}$ switch back to formation control mode. The formation is then achieved after approximately another 15 s. Next, vessel $\mathbf{2}$ detects the dynamic obstacle $\mathbf{o_2}$ and switches to obstacle avoidance mode. After the obstacle is finally cleared at approximately 50 s, vessel $\mathbf{2}$ switches back to formation control mode and then the desired rectangular formation is achieved in about 55 s.

VII. Conclusion

In this work, we present a displacement-based robust formation control and distributed obstacle avoidance framework for *heterogeneous* underactuated surface vessels. The framework is based on the leader–follower model relying only on

relative coordination and thus *without* requiring any global position measurements of either agents or obstacles. Through the generation of feasible trajectories and state transformation, a structured reduced-order error system is developed whose stabilization guarantees convergence of all vehicle states. Then, a supertwisting control design is employed to stabilize the error dynamics. The control law does not require simplification of the vessel dynamics, is not limited to any specific vessel model, and is shown to be robust with respect to modeling uncertainties and bounded disturbances. A distributed obstacle avoidance scheme for the coordinated motion of surface vessel networks is also proposed by surrounding the obstacles with elliptical stable limit cycles, which provide transient trajectories to navigate the vessels around obstacles. It is shown that the network formation continues to persist, albeit in a partially deformed shape, to avoid collision with obstacles or other agents. Numerical simulations are presented to illustrate the effectiveness and robustness of the proposed framework in the presence of disturbances and moving obstacles. The significance of this work is in that it combines robust distributed control of *heterogeneous underactuated* vessel networks without requiring global position measurements, augmented with *distributed obstacle avoidance* capability. Our future research will concentrate on the actuator saturation problem and formation control of three-dimensional vehicles.

APPENDIX

We use this lemma in our proof of Theorems 1 and 2.

Lemma 3 ([32, restated]): Consider the following system:

$$\dot{x}_1 = f(t, x_1) + \omega(t) x_2, \quad \dot{x}_2 = -p\,\omega(t)^\top \left[\frac{\partial V}{\partial x_1}\right]^\top \tag{33}$$

where $x_1 \in \mathbb{R}^{n_1}$, $x_2 \in \mathbb{R}$, $f : \mathbb{R}_{\geq 0} \times \mathbb{R}^{n_1} \to \mathbb{R}^{n_1}$, $\omega : \mathbb{R}_{\geq 0} \to \mathbb{R}^{n_1}$, $V : \mathbb{R}_{\geq 0} \times \mathbb{R}^{n_1} \to \mathbb{R}_{\geq 0}$, and $p > 0$ is a constant. Let the following assumptions A1–A3 hold.

- A1: There exist class $\mathcal{K}_\infty$ functions $\alpha_1(\cdot)$ and $\alpha_2(\cdot)$, and a positive definite function $\alpha_3(\cdot)$ such that, for all $t \geq 0$ and $x_1 \in \mathbb{R}^{n_1}$, $\alpha_1(|x_1|) \leq V(t, x_1) \leq \alpha_2(|x_2|)$, and $\frac{\partial V}{\partial t} + \frac{\partial V}{\partial x_1} f(t, x_1) \leq -\alpha_3(|x_1|)$, a.e.
- A2: There exists continuous nondecreasing function $\beta : \mathbb{R}_{\geq 0} \to \mathbb{R}_{\geq 0}$ such that, for all $t \geq 0$ and $x_1 \in \mathbb{R}^{n_1}$, $\max\{|f(t, x_1)|, |\frac{\partial V(t, x_1)}{\partial x_1}|\} \leq \beta(|x_1|)|x_1|$, a.e.
- A3: The function $\omega(\cdot)$ is bounded, smooth, and PE with a bounded first derivative.

Then, the origin of (33) is UGAS. Moreover, if the origin of system $\dot{x}_1 = f(t, x_1)$ is UGES, then the origin of (33) is UGES.

REFERENCES

[1] Z. Qu, *Cooperative Control of Dynamical Systems: Applications to Autonomous Vehicles*. London, U.K.: Springer-Verlag, 2009.

[2] X. Jin, "Fault tolerant finite-time leader-follower formation control for autonomous surface vessels with LOS range and angle constraints," *Automatica*, vol. 68, pp. 228–236, 2016.

[3] L. Consolini, F. Morbidi, D. Prattichizzo, and M. Tosques, "Leader-follower formation control of nonholonomic mobile robots with input constraints," *Automatica*, vol. 44, no. 5, pp. 1343–1349, 2008.

[4] M. A. Lewis and K.-H. Tan, "High precision formation control of mobile robots using virtual structures," *Auton. Robots*, vol. 4, no. 4, pp. 387–403, 1997.

[5] T. Balch and R. C. Arkin, "Behavior-based formation control for multirobot teams," *IEEE Trans. Robot. Autom.*, vol. 14, no. 6, pp. 926–939, Dec. 1998.

[6] F. Fahimi, "Sliding-mode formation control for underactuated surface vessels," *IEEE Trans. Robot.*, vol. 23, no. 3, pp. 617–622, Jun. 2007.

[7] H. Ashrafiuon, K. Muske, L. McNinch, and R. Soltan, "Sliding-mode tracking control of surface vessels," *IEEE Trans. Ind. Electron.*, vol. 55, no. 11, pp. 4004–4012, Nov. 2008.

[8] W. Dong, "Cooperative control of underactuated surface vessels," *IET Control Theory Appl.*, vol. 4, no. 9, pp. 1569–1580, 2010.

[9] K. Shojaei, "Leader-follower formation control of underactuated autonomous marine surface vehicles with limited torque," *Ocean Eng.*, vol. 105, pp. 196–205, 2015.

[10] J. Ghommam and M. Saad, "Adaptive leader-follower formation control of underactuated surface vessels under asymmetric range and bearing constraints," *IEEE Trans. Veh. Technol.*, vol. 67, no. 2, pp. 852–865, Feb. 2018.

[11] Z. Sun, G. Zhang, Y. Lu, and W. Zhang, "Leader-follower formation control of underactuated surface vehicles based on sliding mode control and parameter estimation," *ISA Trans.*, vol. 72, pp. 15–24, 2018.

[12] T. Li, R. Zhao, C. P. Chen, L. Fang, and C. Liu, "Finite-time formation control of under-actuated ships using nonlinear sliding mode control," *IEEE Trans. Cybern.*, vol. 48, no. 11, pp. 3243–3253, Nov. 2018.

[13] J. Yu, W. Xiao, X. Dong, Q. Li, and Z. Ren, "Practical formation-containment tracking for multiple autonomous surface vessels system," *IET Control Theory Appl.*, vol. 13, no. 17, pp. 2894–2905, 2019.

[14] Y. Lu, G. Zhang, L. Qiao, and W. Zhang, "Adaptive output-feedback formation control for underactuated surface vessels," *Int. J. Control*, vol. 93, no. 3, pp. 400–409, 2020.

[15] T. I. Fossen, *Guidance and Control of Ocean Vehicles*. New York, NY, USA: Wiley, 1994.

[16] K.-K. Oh, M.-C. Park, and H.-S. Ahn, "A survey of multi-agent formation control," *Automatica*, vol. 53, pp. 424–440, 2015.

[17] H.-S. Ahn, *Formation Control: Approaches for Distributed Agents*. Cham, Switzerland: Springer, 2020.

[18] B. Wang, S. Nersesov, and H. Ashrafiuon, "Formation control for underactuated surface vessel networks," in *Proc. ASME Dyn. Syst. Control Conf.*, 2020, Art. no. V002T30A003.

[19] M. Mesbahi and M. Egerstedt, *Graph Theoretic Methods in Multiagent Networks*. Princeton, NJ, USA: Princeton Univ. Press, 2010.

[20] C. A. Desoer and M. Vidyasagar, *Feedback Systems: Input-Output Properties*. Philadelphia, PA, USA: SIAM, 1975.

[21] H. K. Khalil, *Nonlinear Systems*, 3rd ed. Englewood Cliffs, NJ, USA: Prentice-Hall, 2002.

[22] J. A. Moreno and M. Osorio, "Strict Lyapunov functions for the super-twisting algorithm," *IEEE Trans. Autom. Control*, vol. 57, no. 4, pp. 1035–1040, Apr. 2012.

[23] A. Teel, E. Panteley, and A. Loría, "Integral characterizations of uniform asymptotic and exponential stability with applications," *Math. Control Signals Syst.*, vol. 15, no. 3, pp. 177–201, 2002.

[24] Y. Shtessel, C. Edwards, L. Fridman, and A. Levant, *Sliding Mode Control and Observation*. New York, NY, USA: Birkhauser, 2014.

[25] T. I. Fossen, *Marine Control Systems: Guidance. Navigation, and Control of Ships, Rigs and Underwater Vehicles*. Trondheim, Norway: Marine Cybernetics, 2002.

[26] J.-H. Li, P.-M. Lee, B.-H. Jun, and Y.-K. Lim, "Point-to-point navigation of underactuated ships," *Automatica*, vol. 44, no. 12, pp. 3201–3205, 2008.

[27] B. Lu, Y. Fang, and N. Sun, "Continuous sliding mode control strategy for a class of nonlinear underactuated systems," *IEEE Trans. Autom. Control*, vol. 63, no. 10, pp. 3471–3478, Oct. 2018.

[28] J. Huang, S. Ri, T. Fukuda, and Y. Wang, "A disturbance observer based sliding mode control for a class of underactuated robotic system with mismatched uncertainties," *IEEE Trans. Autom. Control*, vol. 64, no. 6, pp. 2480–2487, Jun. 2019.

[29] R. A. Soltan, H. Ashrafiuon, and K. R. Muske, "ODE-based obstacle avoidance and trajectory planning for unmanned surface vessels," *Robotica*, vol. 29, no. 5, pp. 691–703, 2011.

[30] H. Ashrafiuon, S. Nersesov, and G. Clayton, "Trajectory tracking control of planar underactuated vehicles," *IEEE Trans. Autom. Control*, vol. 62, no. 4, pp. 1959–1965, Apr. 2017.

[31] K. R. Muske, H. Ashrafiuon, G. Haas, R. McCloskey, and T. Flynn, "Identification of a control oriented nonlinear dynamic USV model," in *Proc. Amer. Control Conf.*, 2008, pp. 562–567.

[32] E. Panteley, A. Loria, and A. Teel, "Relaxed persistency of excitation for uniform asymptotic stability," *IEEE Trans. Autom. Control*, vol. 46, no. 12, pp. 1874–1886, Dec. 2001.

Bo Wang (Graduate Student Member) received the M.S. degree in control theory and engineering from the University of Chinese Academy of Sciences, Beijing, China, in 2018. He is currently working toward the Ph.D. degree with the Department of Mechanical Engineering, Villanova University, Villanova, PA, USA.

His research interests include nonlinear control theory (robust, adaptive, passive, etc.), underactuated systems, nonholonomic systems, and networked control systems and robotics.

Sergey G. Nersesov (Member, IEEE) received the B.S. and M.S. degrees in aerospace engineering from the Moscow Institute of Physics and Technology, Zhukovsky, Russia, in 1997 and 1999, respectively, and the M.S. degree in applied mathematics and the Ph.D. degree in aerospace engineering both from the Georgia Institute of Technology, Atlanta, GA, USA, in 2003 and 2005, respectively.

He is currently an Associate Professor with the Department of Mechanical Engineering, Villanova University, Villanova, PA, USA. His research interests include nonlinear dynamical system theory, large-scale systems, cooperative control for multi-agent systems, and hybrid and impulsive control for nonlinear systems. He is a coauthor of the books *Thermodynamics. A Dynamical Systems Approach* (Princeton University Press, 2005), *Impulsive and Hybrid Dynamical Systems. Stability, Dissipativity, and Control* (Princeton University Press, 2006), and *Large-Scale Dynamical Systems. A Vector Dissipative Systems Approach* (Princeton University Press, 2011).

Hashem Ashrafiuon (Senior Member, IEEE) received the B.S., M.S., and Ph.D. degrees in mechanical engineering from the State University of New York, Buffalo, NY, USA, in 1982, 1984, and 1988, respectively.

He joined Villanova University, Villanova, PA, USA, faculty after graduating in 1988. He is currently a Professor with the Department of Mechanical Engineering, Villanova University. His research interests include nonlinear control of heterogeneous autonomous vehicles and underactuated systems.

Prof. Ashafiuon is a Fellow of ASME. He is a Senior Editor for the *Journal of Vibration* and has been on the editorial boards of several IEEE and ASME publications.